

Contemporaneous VLBA 5 GHz Observations of LAT-Detected Blazars

J. D. Linford¹, G. B. Taylor¹, R. W. Romani², J. F. Helmboldt³, A. C. S. Readhead⁴, R. Reeves⁴, and J. L. Richards⁴

ABSTRACT

The radio properties of blazars detected by the Large Area Telescope (LAT) on board the *Fermi Gamma-ray Space Telescope* have been observed contemporaneously by the Very Long Baseline Array (VLBA). In total, 232 sources were observed with the VLBA. Ninety sources that were previously observed as part of the VLBA Imaging and Polarimetry Survey (VIPS) have been included in the sample, as well as 142 sources not found in VIPS. This very large, 5 GHz flux-limited sample of active galactic nuclei (AGN) provides insights into the mechanism that produces strong γ -ray emission. In particular, we see that γ -ray emission is related to strong, uniform magnetic fields in the cores of the host AGN. Included in this sample are non-blazar AGN such as 3C84, M82, and NGC 6251. For the blazars, the total VLBA radio flux density at 5 GHz correlates strongly with γ -ray flux. The LAT BL Lac objects tend to be similar to the non-LAT BL Lac objects, but the LAT flat-spectrum radio quasars (FSRQs) are significantly different from the non-LAT FSRQs. Strong core polarization is significantly more common among the LAT sources, and core fractional polarization appears to increase during LAT detection.

Subject headings: galaxies: active - surveys - catalogs - galaxies: jets - galaxies: nuclei - radio continuum: galaxies - gamma-rays: observations

¹Department of Physics and Astronomy, University of New Mexico, MSC07 4220, Albuquerque, NM 87131-0001

²Department of Physics, Stanford University, Stanford, CA 94305

³Naval Research Laboratory, Code 7213, 4555 Overlook Ave. SW, Washington, DC 20375

⁴Astronomy Department, California Institute of Technology, Mail Code 247-17, 1200 East California Boulevard, Pasadena, CA 91125

1. Introduction

The Large Area Telescope (LAT; Atwood et al. 2009) on board the *Fermi Gamma-ray Space Telescope* is a wide-field telescope covering the energy range from about 20 MeV to more than 300 GeV. It has been scanning the entire γ -ray sky once every three hours since July of 2008. The LAT first-year catalog (1FGL; Abdo et al. 2010a) has 1451 sources. The majority of these γ -ray bright sources that have been identified with radio sources are associated with blazars (685 of 1451). These blazars typically are strong, compact radio sources which exhibit flat radio spectra, rapid variability, compact cores with one-sided parsec-scale jets, and superluminal motion in the jets (Marscher 2006).

Several very long baseline interferometry (VLBI) programs, such as the Monitoring Of Jets in AGN with VLBA Experiments (MOJAVE; Lister et al. 2009a; Homan et al. 2009; Lister et al. 2011) observing at 15 GHz, the Boston University program observing at 22 and 43 GHz (Marscher et al. 2010; Jorstad et al. 2010), and TANAMI (Ojha et al. 2010a) observing at 8.4 and 22 GHz, along with the LAT collaboration themselves (Abdo et al. 2011) are in place to monitor the radio jets from the brightest blazars such as 3C273, BL Lac, etc. Our sample has a flux limit roughly an order of magnitude below the MOJAVE survey and so allows us to probe the extensions of the radio core/ γ -ray properties down to a fainter population. Many different radio- γ -ray correlations have been suggested (Taylor et al. 2007, Abdo et al. 2009a, Lister et al. 2009a, Kovalev et al. 2009, Giroletti et al. 2010, Ojha et al. 2010b, Linford et al. 2011). In our last paper (Linford et al. 2011) we found only a marginal correlation between γ -ray flux and radio flux density, and only for the FSRQs. With our new, more contemporaneous and larger sample, we find a strong correlation between the two. By examining a larger sample (1248 objects) we attempt to obtain more definitive insight into several other properties of γ -ray bright blazars.

In Section 2 we define our sample. In Section 3 we briefly describe the data reduction process for our VLBA observations. In Section 4 we present data on the γ -ray flux and radio flux densities of the LAT sources. In Section 5 we discuss differences between sources observed in two epochs (prior to or during 2006 and in 2009 - 2010). In Section 6 we compare several parameters of the LAT and non-LAT sources. Notes on some individual objects of interest are presented in Section 7 and in Section 8 we discuss our results. Throughout this paper we assume $H_0 = 71 \text{ km s}^{-1} \text{ Mpc}^{-1}$ and Λ CDM cosmology (e.g., Hinshaw et al. 2009).

2. Sample Definition

We obtained time on the Very Long Baseline Array (VLBA) to observe LAT-detected sources from November of 2009 to July of 2010. We had a total of 7 observing runs and collected 5 GHz data on 232 sources. The first 3 observing runs were follow-up observations on 90 sources in the VLBA Imaging and Polarimetry Survey (VIPS; Helmboldt et al. 2007) and new 5 GHz observations of 7 sources in the MOJAVE sample. The remaining 135 sources were selected from the Fermi 1FGL as sources which were associated with a source in the Combined Radio All-Sky Targeted Eight GHz Survey (CRATES; Healey et al. 2007) with high ($\geq 80\%$) probability, had a flux density of at least 30 mJy in CRATES, and were not in VIPS or MOJAVE. Of the 232 sources, 95 are BL Lac objects, 107 are FSRQs, and 30 are other types of AGN (radio galaxies, AGN of unknown type, and 1 starburst galaxy). Any object that is not a BL Lac object or FSRQ we classify as ‘AGN/Other’. The optical classifications are taken from the LAT LAT First Catalog of AGN (1LAC; Abdo et al. 2010b). See Table 1 for a summary of our data.

We should note that several of the 1FGL sources are associated with multiple AGN in the 1LAC. Not all of the associated sources are in CRATES, and not all of them are brighter than 30 mJy at 8 GHz. We make a note of those objects with multiple associations in Table 1. We observed 2 radio sources for 3 of the LAT sources in our sample. The LAT source 1FGL J1225.8+4336 is associated with the BL Lac object VIPS J12248+4335 (probability 94%) and the FSRQ VIPS J12269+4340 (probability 87%). The LAT source 1FGL J0448.6+1118 is associated with the FSRQ CRATES J0448+1127 (F04486+112A in our sample; probability 99%) and the BL Lac object PKS 0446+11 (F04486+112B in our sample; probability 92%). The LAT source 1FGL J0510.0+1800 is associated with an AGN of unknown type CRATES J0509+1806 (F05100+180A; probability 91%) and the FSRQ PKS 0507+17 (F05100+180B; probability 100%). It is possible that all of these sources are emitting γ -rays, so we included all of them in our calculations. Where possible, we use the 1LAC redshifts. If the source did not have a redshift listed in 1LAC, we searched the NASA/IPAC Extragalactic Database (NED).

To build a non-LAT detected sample for comparison, we excluded all LAT sources from VIPS, leaving 1018 objects in our non-LAT sample. Of these 1018 objects, 24 are BL Lacs, 479 are FSRQs, and 515 are AGN/Other types (radio galaxies or AGN of uncertain type). The optical types for VIPS sources were adopted from the Candidate Gamma-Ray Blazar Survey (CGRaBS; Healey et al. 2008).

3. VLBA Data Reduction

All VLBA data were correlated using the new DiFX software correlator (e.g., Deller et al. 2011). The correlated data was processed via the VIPS data reduction pipeline using automated scripts. See Taylor et al. (2005) and Helmboldt et al. (2007) for a more thorough description of the VIPS pipeline. Initial calibration (fringe-fitting, flux and phase calibration, polarization calibration) was done using the Astronomical Image Processing System (AIPS; Greisen 2003). Imaging and visibility model-fitting were done using Difmap (Shepherd 1997).

4. Gamma-ray Flux and Radio Flux Density

Throughout the rest of this paper, we will use the nonparametric Spearman test (e.g., Press et al. 1986) to look for correlations between the LAT-detected and non-LAT-detected objects. The Spearman correlation coefficient (ρ_s) has a range of $0 < |\rho_s| < 1$. A high value of ρ_s indicates a significant correlation. This is a powerful test for statistical correlation, but it does not test an actual physical correlation. In order to be certain our correlations are physically significant, we ensure that a redshift selection effect is not adding a bias to our data.

The LAT measures γ -ray flux in several bands. To create total γ -ray fluxes, we combined the fluxes from 3 bands: 100-300 MeV, 300 MeV - 1 GeV, and 1-100 GeV. The fluxes were added and uncertainties were added in quadrature. However, some sources had only upper limits to their fluxes in certain bands. If a source's reported fluxes in one or two bands were upper limits, we use 1/2 the reported flux as the uncertainty in that band as the upper limits are given as 2-sigma results (Abdo et al. 2010a). If a source had upper limits on its flux in all three bands, we adopt the convention of listing its error as 0.00.

4.1. Redshift Selection Effect

Imagine a population of sources covering a wide range of redshifts in which the radio and γ -ray emission is not physically correlated, but in which radio flux and γ -ray flux are correlated with redshift. This is actually what one would naively expect because the more distant objects will be fainter. Such a population will show a strong correlation of radio flux with gamma ray flux via the Spearman test, but this does not indicate a significant physical correlation between these two observables.

However, by investigating the relationship between radio flux density at 5 GHz (S_5)

and redshift for the LAT-detected sources we can rule out a correlation between the two. We calculated the Spearman ρ_s values for the S_5 -z relationship for the BL Lac objects and FSRQs separately. For the BL Lacs, the ρ_s value was 0.308, with a 2.1% probability that random sampling would produce this same ρ_s value. For the FSRQs, the ρ_s value was 0.109, with a 26.2% probability of getting the same value by random sampling. Therefore, there is a very marginal correlation between the radio flux density and redshift for our BL Lac objects, and no correlation for our FSRQs.

We also tested the correlation between γ -ray flux and redshift. The ρ_s values were 0.084 for BL Lacs and 0.016 for FSRQs, with the probability of getting the same values from random sampling of 54.0% and 86.8%, respectively. So, there is no significant correlation between γ -ray flux and redshift for either BL Lac objects or FSRQs. We also visually inspected plots of both LAT flux and total VLBA radio flux density versus redshift and saw no obvious trends, confirming the correlation coefficient results.

4.2. Gamma-ray Flux versus Radio Flux Density

In Fig. 1 we plot the LAT flux versus the total VLBA flux density at 5 GHz. Again, the LAT fluxes are broadband fluxes from 100 MeV to 100 GeV.

The Spearman ρ_s values we found were 0.467 for the BL Lacs and 0.510 for the FSRQs. The probabilities for getting the same ρ_s values from random sampling were 2×10^{-6} for the BL Lac objects and 2×10^{-8} for the FSRQs. Therefore, the LAT flux correlates very strongly with the total VLBA flux density. The BL Lac objects do not correlate quite as strongly, especially considering that we found a marginal correlation between total VLBA flux density and redshift for these objects in the previous section. Still, this provides solid evidence that objects with higher radio flux density also produce more γ -ray flux.

In our previous paper (Linford et al. 2011), we found that there was no strong correlation between radio flux density and γ -ray flux. However, our flux densities for those observations were prior to the launch of *Fermi*. Furthermore, it is likely that the radio flux density increases during episodes of γ -ray flaring (e.g., Kovalev et al. 2009). Our newer, larger, and more contemporaneous set of observations are more appropriate for making these comparisons.

4.3. Radio Flux Density

The median total VLBA flux density at 5 GHz was 177 mJy for the LAT BL Lacs and 221 mJy for the non-LAT BL Lacs. The LAT FSRQ appeared to have significantly higher flux densities than the non-LAT FSRQ, with a median of 467 mJy for LAT FSRQs compared to a median of only 191 mJy for non-LAT FSRQs. The LAT AGN/Other objects also had higher 5 GHz flux densities than their non-LAT sources counterparts. The Kolmogorov-Smirnov (K-S) test probability that the LAT and non-LAT BL Lac objects belong to the same parent population is about 38%. The K-S test probability that the LAT and non-LAT FSRQs are related is only 3×10^{-12} . See Fig. 2 for a plot of the FSRQ total VLBA 5 GHz flux density distributions.

5. Archival versus Contemporaneous

In this section we investigate the changes in the 90 sources that were part of VIPS (i.e., observed in 2006 or earlier) and our new sample (observed in 2009-2010). Of these 90 sources, 35 are BL Lac objects, 44 are FSRQs, and 11 are AGN/other objects. It is important to note that we do not know whether most of our sources were emitting γ -rays in the archival data. It is possible that many of them would have been detected by *Fermi* had it been in operation at the time. Only 6 of these sources were detected by the Energetic Gamma Ray Experiment Telescope (EGRET) on board the *Compton Gamma-ray Observatory* satellite. As an estimate of the uncertainty of the median values we will use the median absolute deviation (MAD) given by

$$MAD(X) = median(|(X_i - median(X))|) \quad (1)$$

where X_i is a value in the array X . In other words, it is the median of the positive difference between each entry in X and the overall median of X . See Huber & Ronchetti (2009) for more information on the MAD.

5.1. Radio Flux Density Variability

It is well known that blazars are highly variable sources in the radio and γ -ray regimes. Several studies have also indicated that the radio and γ -ray variability are correlated (e.g., Kovalev et al. 2009 and Schinzel et al. 2010). Looking at the differences in total VLBA radio flux densities (see Fig. 3) for 90 of our sources that were observed both in 2006 (or earlier) and in 2009, we saw that while there is variability the magnitude of the variability

does not appear to correlate with the γ -ray flux. The median total flux densities showed little significant change between the two epochs. The BL Lac objects had a median flux density of 149.2 mJy in the archival data and 133.2 mJy in the new data. The difference between the medians for the two epochs falls well within the median absolute deviations of 74 mJy for archival data and 72 mJy for the current data. The FSRQs appeared to become somewhat brighter in the new data, with a median flux density of 256.2 mJy in the archival data and 316.0 mJy in the new data. Again, the difference between the two epochs is not significant when compared to the median absolute deviations of 122 mJy for the archival data and 176 mJy for the current data.

We also looked at the radio emission from the core (the bright compact component at the base of the jet). The core flux density was found using automatic visibility fitting (see Taylor et al. 2007 for a more detailed discussion of this process). See Fig. 4 for a plot of the difference in core flux density (current minus archival) versus the total LAT flux. Again, we found that there is no apparent correlation between core flux density variability with LAT flux. The median core flux for the FSRQs is higher during γ -ray detection, going from 225.1 mJy in the archival data to 293.6 mJy in the new data, but this is again within the median absolute deviations of 107 mJy for the archival data and 156 mJy for the new data. Also, from Fig. 4 we can see that most of the FSRQs are actually slightly dimmer, with 25 of the 44 FSRQs showing a reduction in in core flux density.

5.2. Core Brightness Temperature Variability

We obtained the brightness temperatures from automatic model-fitting procedure by fitting to the visibility data directly (Taylor et al. 2007). The minimum observable size for each source was calculated using equation (2) from Kovalev et al. (2005), where we computed the SNR of each core using the core flux density, the rms measured from the 5 GHz image, and a beam FWHM of 3 milliarcseconds (mas), the largest dimension of our restoring beam. For those sources where the estimated core size was less than this minimum size, we used the minimum size to compute the brightness temperature.

The core brightness temperatures are split almost evenly between those that are lower than they were prior to LAT detection and those that are higher. Nearly all had core brightness temperatures in 2009 that were either within 5% of the archival value or higher than the archival value. The median core brightness temperature for the BL Lacs was 2.3×10^{10} K for the archival data and 2.9×10^{10} K for the new data. The median core brightness temperature for the FSRQs in the archival data was 8.2×10^{10} K for and 6.4×10^{10} K for the new data. However, the median absolute deviations were 6.34×10^{10} for the archival data and 5.13×10^{10}

for the new data, so the difference in the medians is not a significant change. See Fig. 5 for a plot of the core flux densities in both epochs.

5.3. Core Polarization Variability

To measure the polarization properties of our sources, we used the Gaussian mask method described by Helmboldt et al. (2007). In order to be considered a “polarized” source, the source had to have a polarized flux of at least 0.3% of the Stokes I peak value (to avoid leakage contamination) and have at least a 5σ detection (compared to the noise image generated by the AIPS task COMB). We obtained measurements of core, jet, and total fractional polarization. Of these, only the core fractional polarization yielded interesting results. We detected polarization in the cores of 80% (72 of 90) of the sources for which we had observations in two epochs. Of our 90 sources, 48 showed higher core fractional polarization in the new data than the archival data. This includes 17 BL Lac objects, 28 FSRQs, and 3 AGN/other objects. Only 15 sources had no polarized flux in their cores in both epochs. Twenty-seven of our sources showed a decrease in core fractional polarization in the new data including 11 BL Lac objects, 12 FSRQs, and 4 AGN/other objects. Of the objects that showed a decrease in core fractional polarization, only 3 (1 BL Lac object and 2 FSRQs) were detected as polarized in the archival data and had no polarized flux in the core in the new data. See Fig. 6 for a plot showing how the core fractional polarizations have changed between the two epochs.

6. LAT Detected versus non-LAT Detected

Throughout this section we compare our large, contemporaneous sample with the non-LAT-detected sources in VIPS.

6.1. Source Classes

We used the automatic classification script from Helmboldt et al. (2007) to classify our sources by appearance for comparison with the VIPS sample. We also went through them by eye and reclassified any objects that the script misidentified. Sources were classified as point sources (PS), short jets (SJET), long jets (LJET), complex (CPLX), or compact symmetric object candidates (CSO). LJET means the source has a jet with an angular extent of at least 6 mas. SJET means the source has a discernible jet, but with an angular extent less

than 6 mas. PS means the source has no discernible jet. CPLX indicates that the source has complicated structure beyond the typical point source or core-jet morphology. See Table 2 for a breakdown of the source classifications for both LAT and non-LAT sources. From this table, it appears that γ -ray bright blazars are more likely to be LJET than the blazars not detected by the LAT. Also, note the lack of CSO candidate objects among the γ -ray bright population. This is something we also reported in Linford et al. (2011).

6.2. Core Brightness Temperature

As discussed in Section 5.2, we obtained the core brightness temperatures by automatic model-fitting to the visibility data. The LAT and non-LAT BL Lac objects were similar, with a median core brightness temperature of 2.89×10^{10} K for the LAT BL Lac objects and 2.65×10^{10} K for the non-LAT. The FSRQs were quite different. The median core brightness temperatures were 6.36×10^{10} K for the LAT FSRQs and 2.54×10^{10} K for the non-LAT FSRQs. The K-S tests show that the LAT FSRQs are indeed very different from the non-LAT FSRQs, with only a 6×10^{-8} chance that the two distributions are drawn from the same parent population. These results confirm those reported in Linford et al. (2011). See Fig. 7 for a plot of the core brightness temperature distributions of LAT and non-LAT FSRQs.

6.3. Jet Brightness Temperature

Unlike the core brightness temperatures, the jet brightness temperatures (formally, the brightness temperature of the brightest jet component) were obtained by automatic model-fitting in the image data. This was done because automatic visibility fitting to jet components has a tendency to go awry for complicated sources. As with the core brightness temperatures, the LAT BL Lac objects were similar to the non-LAT BL Lac objects but the FSRQs appeared to be somewhat different. The K-S test for the FSRQ jet brightness temperature distributions gave probability of 1×10^{-5} that the two were drawn from the same parent population. See Fig. 8 for the distributions of LAT and non-LAT FSRQ jet brightness temperatures. The medians for the FSRQs with measured jet brightness temperatures were 9.8×10^7 K for LAT sources and 4.5×10^7 K for non-LAT sources.

6.4. Jet Opening Angle, Bending, and Length

We measured the mean apparent opening half angle for each source with core-jet morphology. We used the following procedure (Taylor et al. 2007): we measured the separation of each jet component from the core along the jet axis (taken to be a linear fit to the component positions) and the distance of each component from the jet axis, i.e., x' and y' positions in a rotated coordinate system with the jet axis along the x' -axis. For each component, we measured its extent from its center along a line perpendicular to the jet axis using the parameters of its elliptical fit, and then deconvolved this using the extent of the Gaussian restoring beam along the same line. The opening half-angle measured from each component is then taken to be

$$\psi = \arctan[(|y'| + dr)/|x'|] \quad (2)$$

where dr is the deconvolved Gaussian size perpendicular to the jet axis. After measuring this for each jet component, we averaged them to get a single value. This was only done for sources with more than 2 total components, (i.e., at least 2 jet components).

The K-S tests for the LAT and non-LAT distributions found no significant differences between the two for any of the optical types. However, we noticed that our LAT sources have large apparent opening angles (≥ 30 degrees) more often than the non-LAT sources, 37% of LAT sources versus 28% of non-LAT sources. See Fig. 9 for plots of the opening angle distributions. Pushkarev et al. (2009) also reported that LAT-detected MOJAVE sources in the 3 month LAT catalog tended to have larger opening angles than non-LAT sources. Ojha et al. (2010b) reported a tentative correlation between opening angle and γ -ray flux. We did not find any strong evidence of this. Using the Spearman test on all 49 of our sources with measured opening angles, we got a ρ_s value of 0.2 and probability of getting the same ρ_s value from random sampling of 16%. Looking at the FSRQs alone, we found a ρ_s of 0.5 and a 1.4% probability of getting the same result from random sampling. Therefore, there may be a marginally significant correlation between γ -ray flux and opening angles for FSRQs. Also, the K-S test result for the LAT and non-LAT FSRQs gave a 6.4% chance that the two distributions are drawn from the same parent sample. The BL Lacs showed no significant correlation and no significant difference between the LAT and non-LAT distributions.

In order to make a larger sample for the K-S test, we combined the BL Lac objects and FSRQs into one sample. The result was a marginally significant difference between the LAT and non-LAT sources. The K-S test result was a 0.4% chance that the two distributions were drawn from the same parent population. We also applied the Spearman test on this sample to look for correlation with LAT flux. We did not find significant correlation, with a ρ_s value of 0.3 and a probability of getting the same ρ_s value from random sampling of 9%.

Lister et al. (2011) reported a non-linear correlation between γ -ray loudness (the ratio of γ -ray luminosity to radio luminosity) and apparent opening angle. They also found that all 19 of their sources with the large ($>40^\circ$) apparent opening angles had a γ -ray loudness of more than 100. They did not find a significant difference in the opening angle distributions between BL Lac objects and FSRQs. We are currently investigating these quantities in our data and we will report our results as soon as possible.

We also measure the change in jet position angle (“jet bending”, see Helmboldt et al. 2008) and the length of the jet (the maximum separation between the core component and the jet components). We applied the K-S test to each of these measurements to see if the LAT and non-LAT distributions were different. We did not find any significant differences for either of these properties.

6.5. Polarization

We measured the polarization characteristics of our sources the same way as described in Section 5.3. As discussed therein, a source is considered to be polarized if it has a polarized flux of at least 0.3% of the Stokes I peak and at least a 5σ detection. For the LAT sources, 176 of 232 (about 76%) showed core polarization. The FSRQs had the highest percentage of polarized sources with 96 of 107 (90%). The BL Lac objects had 67 of 95 (71%) sources with core polarization, and the AGN/other sources had 13 of 30 (43%) sources with core polarization. Compare these numbers with the non-LAT VIPS sources where only 270 of 1018 (26.5%) had core polarization. For the non-LAT sample, the BL Lac objects were polarized most often, but only 10 of 24 (42%). The non-LAT FSRQs had 158 out of 479 (33%) sources with core polarization, and the AGN/other only had 102 of 515 (20%).

Despite the LAT sources having polarized cores more often, they do not appear to be more strongly polarized. The median core fractional polarization is 3.7% for LAT BL Lac objects and 3.1% for LAT FSRQs. The non-LAT sample has higher medians, with 4.9% for BL Lac objects and 3.7% for FSRQs. Overall, the median core fractional polarization for the LAT sample is 3.3% while the median for the non-LAT sample is 4.4%. The K-S test showed no significant differences between the LAT and non-LAT BL Lac or AGN/other objects. There is a marginally significant result for the FSRQs, with a probability of 0.2% that the LAT and non-LAT FSRQs were drawn from the same parent population. We plot the distribution of core fractional polarization for the FSRQs in Fig. 10.

7. Notes on Individual Sources

In this section we present information on low redshift ($z < 0.02$) sources and non-blazar AGN in our sample. Contour maps of these sources are shown in Fig. 11, except for F03197+4130 (a.k.a. 3C84) as it is a very well-known source.

7.1. Low Redshift Objects

Our sample contains 3 objects with redshifts of $z < 0.02$.

F03197+4130, 1FGL J0319.7+4130, class LJET: This well known radio galaxy, 3C84, has a redshift of $z = 0.018$ (1LAC). Its LAT flux was 213.59 ± 10.69 photons $\text{cm}^{-2} \text{s}^{-1}$. We measured a total VLBA flux density of 16.2 Jy. Its core brightness temperature was 1.23×10^{11} K, which is relatively high for the AGN/Other objects. We did not detect any polarized flux from this object. This lack of strong polarization is well known and attributed to a Faraday screen consisting of the ionized gas which also produces the $\text{H}\alpha$ in the Perseus cluster (Taylor et al. 2006). It has a jet and counterjet aligned north-south, with the northern jet showing significant free-free absorption (Walker et al. 2000). We measured the southern jet to be about 15.8 mas long. The northern counterjet had one dim component located about 11.8 mas from the core. No contour map for this source is provided here as it is a very famous source.

F09565+6938, 1FGL J0956.5+6938, class PS: With a redshift of $z=0.000677$ (de Vaucouleurs et al. 1991), the starburst galaxy M82 is 1 of 2 starburst galaxies in the 1FGL. It had a LAT flux of 38.40 ± 16.23 photons $\text{cm}^{-2} \text{s}^{-1}$. We found a total VLBA flux density of 14 mJy. Its core brightness temperature was a relatively low 3.39×10^9 K. We did not detect any polarization for this object. In the optical, this galaxy has a very striking x-shape with bright filaments running perpendicular through a spiral disk (e.g., Mutchler et al. 2007). At 5 GHz, it is simply a point-source. It is also thought to host two intermediate mass (12,000 to 43,000 M_\odot) black holes (Feng, Rao, & Kaaret 2010).

F17250+1151, 1FGL J1725.0+1151, class SJET: This BL Lac object, also known as CRATES J1725+1152, has a redshift of $z = 0.018$ (Ciliegi, Bassani, & Caroli 1993). Its LAT flux was 54.96 ± 23.25 photons $\text{cm}^{-2} \text{s}^{-1}$. We measured a total VLBA flux density of 63.3 mJy. Its core fractional polarization was 3.5%. It is a compact source with a short jet extending about 3.5 mas to the southeast.

7.2. AGN

The LAT 1FGL contains 28 sources which are classified as “AGN”, which means “other non-blazar AGN” (Abdo et al. 2010a). We have 12 of these objects in our sample. (Note: 1FGL J0319.7+4130, a.k.a. 3C 84, is discussed above as a low-redshift object.) Some of the objects in this section are radio galaxies, but others may be misidentified FSRQs and BL Lac objects.

J09235+4125, 1FGL J0923.2+4121, class LJET: Also known as CRATES J0923+4125, this object had a LAT flux of 40.61 ± 10.01 photons $\text{cm}^{-2} \text{s}^{-1}$. Its redshift is $z=0.028$ (1LAC). This object was observed in two epochs; first in May 2006 and second in November of 2009. In 2006, we found a total VLBA flux density of 165 mJy. In 2009, we found a total VLBA flux density of 220 mJy. While its core brightness temperature is not unusually high or low for AGN/Other objects, it did change significantly between the two epochs. In 2006, its core brightness temperature was 4.91×10^9 K. In 2009, we found a core brightness temperature of 2.97×10^{10} K. We detected polarization in the core of this object in both epochs. In 2006, its core fractional polarization was 5.2%. In 2009, its core fractional polarization was 3.1%. We also detected polarization in the jet in 2009, with a jet fractional polarization of 18.3%. For more discussion on this object, see Linford et al. (2011). It has a jet extending about 9.7 mas to the east.

J12030+6031, 1FGL J1202.9+6032, class LJET: Also known as CRATES J1203+6031, this object had a LAT flux of 44.79 ± 10.07 photons $\text{cm}^{-2} \text{s}^{-1}$. Its redshift is $z=0.065$ (1LAC). This object was observed in two epochs; first in May of 2006 and second in December of 2009. Its total VLBA flux density did not change much between the two epochs, but it did show an increase in core brightness temperature. In 2006, its core brightness temperature was 7.22×10^9 . In 2009, we found a core brightness temperature of 2.75×10^{10} K. It had strong core polarization in both epochs. In 2006, we found a core fractional polarization of 9.9%. In 2009, we found a core fractional polarization of 4.8%. For more discussion on this object, see Linford et al. (2011). It has a long jet extending about 10.5 mas to the south.

J13307+5202, 1FGL J1331.0+5202, class LJET: This object is also called CRATES J1330+5202. Its LAT flux was 41.52 photons $\text{cm}^{-2} \text{s}^{-1}$, but is an upper limit. It has a redshift of 0.688 (1LAC). This object was observed in two epochs; first in July of 2006 and second in January of 2010. Its total VLBA flux density and core brightness temperature did not change significantly between the two epochs. We did not detect any polarization from this object in either epoch. For further discussion on this object, see Linford et al. (2011). It has a small jet extending about 7 mas to the southwest.

J16071+1551, 1FGL 1607.1+1552, class LJET: Also called NVSS J160706+155134,

its LAT flux was 33.90 ± 7.75 photons $\text{cm}^{-2} \text{s}^{-1}$. Its redshift is $z=0.496$ (1LAC). It is called a BL Lac object in Véron-Cetty & Véron (2006). This object was observed in two epochs; the first in April 2006 and the second in January 2010. In 2006, we measured a total VLBA flux density of 281 mJy. In 2010, we measured a total VLBA flux density of 322 mJy. It is a strongly polarized source in both epochs. We measured a core fractional polarization of 3.5% in 2006 and 4.5% in 2010. We also found polarization in the jet in both epochs. In 2006 we measured a jet fractional polarization of 15.5%, and in 2010 we measured 24%. For more information, see Linford et al. (2011). It has a long jet extending about 10 mas to the east.

J16475+4950, 1FGL J1647.4+4948, class LJET: Also called CRATES J1647+4950, this object had a LAT flux of 33.29 ± 8.54 photons $\text{cm}^{-2} \text{s}^{-1}$. It has a redshift of $z=0.047$ (1LAC). This object was observed in two epochs; first in August of 2006 and second in January of 2010. Its total VLBA flux density and core brightness temperature did not change significantly between those two epochs. We did not detect any significant core polarization in this object in either epoch, but we did measure 27.1% jet polarization in 2010. For more information on this object, see Linford et al. (2011). It has a small jet extending about 7 mas to the southeast.

J17240+4004, 1FGL J1724.0+4002, class LJET: This object is also called CRATES J1724+4004. Its LAT flux was 47.16 ± 8.97 photons $\text{cm}^{-2} \text{s}^{-1}$. Its redshift is $z=1.049$ (1LAC). It is tentatively classified as a BL Lac object in Véron-Cetty & Véron (2006). This object was observed in two epochs; first in February 1998 and second in January 2010. Its total VLBA flux density did not change significantly between the two epochs, but its core brightness temperature more than doubled. In 1998, its core brightness temperature was 6.08×10^{10} . In 2010, we found a core brightness temperature of 3.32×10^{11} K, which is the highest core brightness temperature for the “AGN” objects in our sample. We did not detect any polarization in this object in either epoch. For further discussion of this object, see Linford et al. (2011). It has a long jet extending 9 mas to the northwest.

F02045+1516, 1FGL J0204.5+1516, class LJET: This object is also known as 4C +15.05, and it is often classified as an FSRQ (Véron-Cetty & Véron 2006, Savolainen et al. 2010, Agudo et al. 2010). Its LAT flux was 29.98 ± 12.42 photons $\text{cm}^{-2} \text{s}^{-1}$. We measured a total VLBA flux density of 1.5 Jy. Its redshift is $z=0.405$ (1LAC). Its core brightness temperature was a relatively high 9.52×10^{10} K. We did not detect any polarization from this object. This is one of the sources monitored as part of the MOJAVE program. Savolainen et al. (2010) reported an apparent velocity of 6.3c, a Doppler factor of 15.0, and a Lorentz factor of 8.9. It has a bright jet component about 7 mas northwest of the core.

F03250+3403, 1FGL J0325.0+3402, class LJET: Also called CRATES J0324+3410,

this object is a Seyfert 1 galaxy (Abdo et al. 2009b). It had a LAT flux of 56.29 ± 23.97 photons $\text{cm}^{-2} \text{s}^{-1}$. We measured a total VLBA flux density of 357 mJy. It has a redshift of $z=0.061$ (1LAC). We detected polarization in both the core and jet of this object. Its core fractional polarization was 1.0% and its jet fractional polarization was 33.4%. Zhou et al. (2007) reported the existence of spiral arm structure in this object based on *Hubble Space Telescope* images. Antón et al. (2008), using the Nordic Optical Telescope, suggested that the apparent structure could be the result of a merger. In the radio, it has a long straight jet extending about 9.6 mas to the southeast.

F16354+8228, 1FGL J1635.4+8228, class LJET: This object is also known as NGC 6251. It is an unabsorbed Seyfert 2, meaning it has a X-ray hydrogen column density $N_H \leq 10^{22} \text{ cm}^{-2}$ and does not have a broad line region (Panessa & Bassani 2002). It is a well-known radio source with an exceptionally long (about 200 kpc) and straight jet (Waggett, Warner, & Baldwin 1977) and is popularly known as the “blowtorch” jet. Its LAT flux was 45.51 ± 18.77 photons $\text{cm}^{-2} \text{s}^{-1}$. We measured a total VLBA flux density of 637 mJy. Its redshift is $z=0.025$ (1LAC). We did not detect any polarization in this object, although it has been reported to be weakly polarized (Chen et al. 2011). It has a long straight jet extending about 8.5 mas to the northwest.

F16410+1143, 1FGL J1641.0+1143, LJET: Also called NVSS J164058+114404, this object had a LAT flux of 47.36 ± 20.81 photons $\text{cm}^{-2} \text{s}^{-1}$. We measured a total VLBA flux density of 115 mJy. It has a redshift of 0.078 (1LAC). We found a core brightness temperature of $1.65 \times 10^9 \text{ K}$, which is the lowest of the “AGN” type objects. We did not detect any polarization for this object. In the CRATES catalog, it is called a flat-spectrum radio source (Healey et al. 2007). It has a jet extending about 10 mas to the west, ending in a semi-detached component.

F17566+5524, 1FGL J1756.6+5524, class LJET: This object is also called CRATES J1757+5523. It had a LAT flux of 27.79 ± 12.00 photons $\text{cm}^{-2} \text{s}^{-1}$. We measured a total VLBA flux density of 47 mJy. Its redshift is 0.065 (1LAC). In the CRATES catalog, it is called a flat-spectrum radio source (Healey et al. 2007). We did not detect any polarized flux from this object. It has a jet stretching about 8 mas to the north-northwest.

7.3. AGN with No Optical ID

Many sources in the LAT catalog are labeled as “AGU” sources, which means “active galaxy of uncertain type” (Abdo et al. 2010a). These sources are associated with radio AGN, but have no optical identification as yet. We have 16 of them in our sample. It is

likely that most of them are FSRQs.

J11061+2812, 1FGL J1106.5+2809, class PS: This object is also called CRATES J1106+2812. The CRATES catalog lists it as a flat-spectrum radio source (Healey et al. 2007). It had a LAT flux of 34.63 ± 15.03 photons $\text{cm}^{-2} \text{s}^{-1}$. It has a redshift of 0.847 (Adelman-McCarthy et al. 2008). This object was observed in two epochs; first in February 2006 and second in December 2009. In 2006, we found a total VLBA flux density of 276 mJy, and in 2009 we measured a total VLBA flux density of 227 mJy. Its core brightness temperature more than doubled between the two epochs, going from 5.08×10^{10} K in 2006 to very high 2.25×10^{11} K in 2009. In fact, this object had the highest core brightness temperature of all the “AGU” objects in our sample. We detected polarization in the core of this object in both epochs. In 2006, we measured a core fractional polarization of 1.4%, and in 2009 its core fractional polarization was 4.4%. For more discussion on this object, see Linford et al. (2011). It is a compact, point-source type object.

J11421+1547, 1FGL J1141.8+1549, class LJET: This object is also called CRATES J1142+1547. The CRATES catalog lists it as a flat-spectrum radio source (Healey et al. 2007). It had a LAT flux of 12.87 ± 5.19 photons $\text{cm}^{-2} \text{s}^{-1}$. There is no published redshift for this object. This object was observed in two epochs; first in February 2006 and second in December 2009. Its total VLBA flux density was 172 mJy in 2006 and 139 mJy in 2009. Its core brightness temperature increased between the two epochs from 5.62×10^{10} K to 9.15×10^{10} K, which is high for an AGN/Other type object. We detected polarization in the core of this object in both epochs. In 2006, the core fractional polarization was 6.3% and in 2009 the core fractional polarization was 5.5%. We also detected polarization in the jet in 2009. The jet fractional polarization was 31.1%. For more information on this object, see Linford et al. (2011). It has a jet extending about 11.5 mas to the southeast.

J12248+4335 (class LJET) & J12269+4340 (class SJET), 1FGL J1225.8+4336: The LAT source 1FGL J1225.8+4336, with a LAT flux of 36.15 ± 15.51 photons $\text{cm}^{-2} \text{s}^{-1}$, is associated with two VIPS sources, both of which were observed in two epochs; first in May 2006 and second in December 2009. First, J12248+4335 (probability: 94%, 1LAC), also called NVSS J122451+433520. This object is called a BL Lac object by Plotkin et al. (2008) but listed as an “Unknown” type in both 1FGL and 1LAC. It has a redshift of $z=1.07491$ (Sowards-Emmerd, Romani, & Michelson 2003). In 2006, we measured a total VLBA flux density of 174 mJy and in 2009 we measured a total VLBA flux density of 207 mJy. Its core brightness temperature increased from 1.80×10^{10} K in 2006 to 3.15×10^{10} K in 2009. We also detected polarization in the core and jet of this object in both epochs. In 2006, its core fractional polarization was 7% and its jet fractional polarization was 18%. In 2009, its core fractional polarization was 5.4% and its jet fractional polarization was 42.6%. It

has a jet extending about 8 mas to the northeast. Second, J12269+4340 (probability: 87%, 1LAC), or CRATES J1226+4340, is a FSRQ (Véron-Cetty & Véron 2006 and 1LAC). It has a redshift of $z=2.002$ (1LAC). Its total VLBA flux density and core brightness temperature did not change significantly between the two epochs. We detected core polarization only in the 2009 observation. We found core fractional polarization of 4.2%. It is a compact source with a possible jet extending about 5.6 mas to the south.

J13338+5057, 1FGL J1333.2+5056, class PS: This object, also called CLASS J1333+5057, has no published classification. Its LAT flux was 64.33 ± 27.63 photons $\text{cm}^{-2} \text{s}^{-1}$. It has a redshift of $z = 1.362$ (Abdo et al. 2009). It was observed in two epochs; first in August 2006 and second in January 2010. It was very dim in 2006, with a total VLBA flux density of 40 mJy, but it doubled to 80.2 mJy in 2010. Its core brightness temperature also increased by about a factor of 2 from 6.24×10^9 K in 2006 to 1.46×10^{10} K in 2010. We did not detect any polarization in this object in either epoch. It is a compact, point-source type object.

F03546+8009, 1FGL J0354.6+8009, class LJET: This object is also known as CRATES J0354+8009. The CRATES catalog lists it as a flat-spectrum radio source (Healey et al. 2007). Its LAT flux was 46.05 ± 8.82 photons $\text{cm}^{-2} \text{s}^{-1}$. We measured a total VLBA flux density of 280 mJy. There is no published redshift for this object. It was a very strongly polarized source with a core fractional polarization of 14.2%. It has a broad, diffuse jet extending about 9.8 mas to the southeast. It also had a large opening angle of 35° . Britzen et al. (2008) measured the kinematics of two of the jet components for this object and found apparent velocities of $0.007c$ for the one nearer the core and $0.064c$ for the one further from the core.

F05100+180A&B (both class LJET), 1FGL J0510.0+1800: The LAT source 1FGL J0510.0+1800, with a LAT flux of 33.38 ± 12.39 photons $\text{cm}^{-2} \text{s}^{-1}$, is associated with 2 of our radio sources. The first, F05100+180A, is also known as CRATES J0509+1806. In 1LAC, its optical type is listed as “Unknown”. The CRATES catalog lists it as a flat-spectrum radio source (Healey et al. 2007). It has no published redshift. We measured a total VLBA flux density of 44.8 mJy. We did not detect any polarized flux from this object. It has a long jet extending to the east with a detached component about 16 mas from the center of the core. The second radio source, F05100+180B, is a FSRQ also known as PKS 0446+17. We measured a total VLBA flux density of 441 mJy. We detected polarized flux in both the core and jet of this object. Its core fractional polarization was 3.8% and its jet fractional polarization was 12.8%. It has a long jet extending about 13 mas to the west.

F06544+5042, 1FGL J0654.4+5042, class SJET: This object is also called CRATES J0654+5042. The CRATES catalog lists it as a flat-spectrum radio source (Healey et al. 2007). Its LAT flux was 42.02 ± 7.63 photons $\text{cm}^{-2} \text{s}^{-1}$. Abdo et al. (2010c) report that its

γ -ray flux ($E > 300$ MeV) is variable. We measured a total VLBA flux density of 240 mJy. It has no published redshift. We found a core fractional polarization of 8.1%. It has a small jet extending about 4.7 mas to the east.

F08499+4852, 1FGL J0849.9+4852, class LJET: This object is also known as CRATES J0850+4854. The CRATES catalog lists it as a flat-spectrum radio source (Healey et al. 2007). Its LAT flux was 29.87 ± 6.99 photons $\text{cm}^{-2} \text{s}^{-1}$. We measured a total VLBA flux density of 60.1 mJy. There is no published redshift for this object. We found a core brightness temperature of 1.20×10^9 K, which is the lowest of all the AGN/Other type objects. We did not detect any polarization in this object. It has a small jet extending about 8 mas to the south. It also has a large opening angle of 54.2° .

F09055+1356, 1FGL J0905.5+1356, class SJET: This object is also called CRATES J0905+1358. The CRATES catalog lists it as a flat-spectrum radio source (Healey et al. 2007). Its LAT flux was 18.39 ± 7.21 photons $\text{cm}^{-2} \text{s}^{-1}$. We measured a total VLBA flux density of 48.5 mJy. It has no published redshift. We did not detect any polarization in this object. It is a compact object with a very short jet extending about 1.3 mas to the west.

F09498+1757, 1FGL J0949.8+1757, class SJET: This object is also known as CRATES J0950+1804. The CRATES catalog lists it as a flat-spectrum radio source (Healey et al. 2007). It had an upper limit on its LAT flux of 18.85 photons $\text{cm}^{-2} \text{s}^{-1}$. We measured a total VLBA flux density of 37.2 mJy. Its redshift is 0.69327 (Adelman-McCarthy et al. 2008). We did not detect any polarized flux from this object. It appears to have a short jet extending about 5 mas to the east.

F10485+7239, 1FGL J1048.5+7239, class LJET: This object is also known as CRATES J1047+7238. The CRATES catalog lists it as a flat-spectrum radio source (Healey et al. 2007). Its LAT flux was 44.18 ± 19.09 photons $\text{cm}^{-2} \text{s}^{-1}$. We measured a total VLBA flux density of 61 mJy. It has no published redshift. We found a core fractional polarization of 5.2%. It has a jet extending about 12 mas to the west.

F13060+7852, 1FGL J1306.0+7852, class SJET: This object is also called CRATES J1305+7854. The CRATES catalog lists it as a flat-spectrum radio source (Healey et al. 2007). Its LAT flux was 17.53 ± 6.82 photons $\text{cm}^{-2} \text{s}^{-1}$. We measured a total VLBA flux density of 213 mJy. There is no published redshift for this object. We found a core fractional polarization of 4.2%. It has a small jet extending about 5 mas to the northeast.

F13213+8310, 1FGL J1321.3+8310, class LJET: This object is also called CRATES J1321+8316. The CRATES catalog lists it as a flat-spectrum radio source (Healey et al. 2007). Its LAT flux was 27.88 ± 11.62 photons $\text{cm}^{-2} \text{s}^{-1}$. We measured a total VLBA flux density of 232 mJy. It has a redshift of $z=1.024$ (Britzen et al. 2007). We did not

detect any polarization in this object. It has a long, diffuse jet extending about 22.5 mas to the west. It also appears to have an older, detached jet component about 33 mas to the southwest. Britzen et al. (2008) had measurements for the kinematics on two components in this source’s jet, but for some reason they did not use the redshift quoted earlier. Using that redshift, and Britzen’s total proper motions of $0.041 \text{ mas yr}^{-1}$ for the component nearer to the core and $0.127 \text{ mas yr}^{-1}$ for the component further from the core, we find apparent velocities of $1.08c$ and $3.35c$, respectively.

F19416+7214, 1FGL J1941.6+7214, class SJET: This object is also called CRATES J1941+7221. There is no published classification for it. Its LAT flux was 66.46 ± 29.70 photons $\text{cm}^{-2} \text{ s}^{-1}$. We measured a total VLBA flux density of 775 mJy. There is no published redshift for this object. We did not detect any polarization in this object. It has a small jet extending about 4 mas to the south.

F20019+7040, 1FGL J2001.9+7040, class LJET: This object is also known as CRATES J2001+7040. The CRATES catalog lists it as a flat-spectrum radio source (Healey et al. 2007). Its LAT flux was 27.18 ± 10.17 photons $\text{cm}^{-2} \text{ s}^{-1}$. We measured a total VLBA flux density of 36.5 mJy. There is no published redshift for this object. We did not detect any polarization in this object. It has a long, diffuse jet extending about 14 mas to the north.

F20497+1003, 1FGL J2049.7+1003, class LJET: This object is also known as CRATES J2049+1003. It may also be the EGRET source 3EG J2046+0933 (Bloom 2008). The CRATES catalog lists it as a flat-spectrum radio source (Healey et al. 2007). Its LAT flux was 58.69 ± 25.99 photons $\text{cm}^{-2} \text{ s}^{-1}$. We measured a total VLBA flux density of 698 mJy. It has no published redshift. We found a core brightness temperature of $6.07 \times 10^{10} \text{ K}$. We found a very low core fractional polarization of 0.8%. It has a jet extending about 6.3 mas to the northwest.

7.4. Unidentified Sources

Our sample contains 2 objects for which no optical classification is given in the 1FGL catalog.

J09292+5013, 1FGL J0929.4+5000, class LJET: In our previous paper (Linford et al. 2011), we identified this source as a BL Lac object. It is associated with the BL Lac object VIPS J09292+5013 (CRATES J0929+5013), but with a low probability (67%, 1LAC). For this paper, we treated it as a BL Lac object. It had a LAT flux of 21.40 ± 9.29 photons $\text{cm}^{-2} \text{ s}^{-1}$. The two epochs for which we have observations of this object are February 1998 and November 2009. It has a redshift of $z=0.370387$ (Adelman-McCarthy et al. 2005). Its

total VLBA flux density did not change significantly between the two epochs. In 1998, we found a core brightness temperature of 6.67×10^{10} K, and in 2009 we found a core brightness temperature of 4.81×10^{10} K. Even with this somewhat reduced core brightness temperature, it was still in the upper 33% of BL Lac objects in the current sample. It was a strongly polarized source with a core fractional polarization of 16.9%.

J11540+6022, 1FGL J1152.1+6027, class PS: This is associated with VIPS J11540+6022 (CRATES J1154+6022), a source of unknown type, with a probability of 73% (1LAC). Healey et al. (2007) call it a flat-spectrum radio source. Its LAT flux was 46.21 ± 20.76 photons $\text{cm}^{-2} \text{s}^{-1}$. We measured a total VLBA flux density of 232 mJy. It has no published redshift. We found a core brightness temperature of 3.93×10^{11} K, which is the highest core brightness temperature of all the “Other” type objects and the 16th highest in our entire sample. We found a core fractional polarization of 1.4%.

8. Discussion and Conclusions

8.1. Polarization and Magnetic Fields

The widely accepted picture of AGN central engine is a spinning super-massive black hole surrounded by an accretion disk (Blandford 1976, Lovelace 1976, Urry & Padovani 1995). In order to launch and collimate the jets, most models include a strong magnetic field which is coiled into a helical shape by the rotation of the accretion disk or the black hole. Meier (2005) proposed a model where the magnetic field lines originate in the accretion disk and then thread through the ergosphere (the region near a rotating black hole where spacetime itself is rotating as a result of frame dragging) of the rotating central black hole. This allows for the black hole to tightly wind the magnetic field lines, leading to reconnection events which can launch fast-moving material. This may be the source of the γ -ray emitting regions in our blazars.

We know that strong, uniform magnetic fields lead to polarized emission. Because the majority (76%) of our γ -ray bright sources showed significant polarization in their cores, it is obvious that they have strong, well-ordered magnetic fields in their centers. The fact that the non-LAT sources are polarized less often (see Fig. 12) leads us to believe that the strong, uniform magnetic fields are somehow tied to the γ -ray emission. Also, recall from Section 5.3 that the core fractional polarization appeared to increase during LAT detection. Furthermore, Abdo et al. (2010d) noted a dramatic change in the optical polarization orientation angle coincided with strong γ -ray emission in 3C279. A possible explanation for this is that the magnetic fields in the cores become stronger (field lines wound more tightly)

and more uniform (lines pulled into a less chaotic configuration) when γ -ray emission occurs. In other words, following from the model in Meier 2005 discussed above, the spinning black hole winds up the magnetic fields lines until there is a reconnection event which launches a new, fast-moving jet component. This new component upscatters background photons to GeV energies via inverse Compton processes (e.g., Björnsson 2010, Tavecchio et al. 2011, Abdo et al. 2011). Meier (2005) expected several reconnection events in succession, followed by a time when the field has pulled back from the black hole. Thus, the objects for which we do not detect polarization in the core could be in the state where the field is not being wound up by the black hole.

8.2. Opening Angles

While we did not have a large sample of objects with measured opening angles, we did find a hint that the LAT and non-LAT distributions are different. The K-S test gave a 0.4% probability that the LAT and non-LAT distributions of BL Lac object and FSRQ opening angles are taken from the same parent sample. This is not a highly significant result, but it is tantalizing in view of what other studies have reported (e.g., Pushkarev et al. 2009; Ojha et al. 2010b; Lister et al. 2011).

8.3. BL Lac Objects

The only significant difference between the LAT and non-LAT BL Lac objects was that the LAT BL Lacs are polarized more often. However, 10 of the 24 non-LAT BL Lac objects showed significant core polarization, so core polarization itself is not enough to separate the two populations. It seems likely, therefore, that all BL Lacs produce γ -rays, but we simply do not detect all of them with the LAT. It is well known that BL Lac objects are highly variable sources in radio and γ -ray bands (Abdo et al. 2011). It is possible that LAT does not detect some BL Lac objects because they have lower than average Doppler factors, either as a result of lower velocities and/or jet orientations further from the line-of-sight. Lister et al. (2009c) measured the kinematics of both LAT and non-LAT BL Lac objects, and found two non-LAT BL Lac objects with maximum jet material speeds higher than the LAT BL Lac objects. However, they only had 21 BL Lac objects, 10 of which were LAT-detected. Further study of BL Lac object kinematics is needed before we can claim LAT BL Lacs tend to have higher bulk material velocities. It is also possible that BL Lac objects occasionally enter a state where γ -ray production ceases or is at least significantly reduced. This question may be answered with continued monitoring of BL Lac objects with LAT and future instruments.

8.4. FSRQs

The LAT FSRQs exhibited several significant differences from the non-LAT FSRQs. The LAT FSRQs had higher radio flux densities, higher core brightness temperatures, and were polarized much more often than the non-LAT FSRQs. The LAT FSRQs also seemed to have higher jet brightness temperatures, although this is a marginal result. It is also possible that the LAT FSRQs have larger opening angles than non-LAT FSRQs, but this result is tentative and is not strongly supported by the K-S test.

As with the BL Lac objects, we saw significant variation in flux density, core brightness temperature, and core polarization for those sources for which we had two epochs of observations. However, as a group the FSRQs did not change significantly in flux density or core brightness temperature between the two epochs. We did find an increase in the number of sources with strong core polarization.

About 90% (96 of 107) of the LAT FSRQs showed significant polarization in their cores. Compare this with only about 33% of the non-LAT FSRQs showing core polarization, and we can see that core polarization is a strong indicator of γ -ray emission. Of the 44 FSRQs for which we had observations in two epochs, 28 showed higher core fractional polarization during LAT detection. Only 12 showed a decrease in core fractional polarization. So, it appears that the cores of FSRQs tend to become more polarized during LAT detection.

8.5. Other Non-Blazar AGN

We found two significant differences between the LAT and non-LAT non-blazar AGN. The first is the total radio flux density. The LAT non-blazar AGN tended to have higher flux density than their non-LAT counterparts. The K-S test resulted in a 8.8×10^{-4} chance that the LAT and non-LAT distributions are drawn from the same parent distribution. Second, the LAT non-blazar AGN are polarized much more frequently. We detected polarization in about 43% (13 of 30) of our LAT sources, compared to only about 20% (102 of 515) for our non-LAT sample. As with the BL Lac objects and FSRQs, the non-blazar AGN are not necessarily more strongly polarized, but polarized more often.

Also, there remains a definite lack of CSO candidates among LAT-detected AGN, despite some predictions to the contrary (e.g., Stawarz et al. 2008).

We thank the anonymous referee for helpful comments on the manuscript. We thank Steve Tremblay and Marcello Giroletti for their helpful advice and comments. We also thank Steve Myers and Josh Marvil for their help with obtaining EVLA observations of

several sources for polarization angle calibration. The National Radio Astronomy Observatory is a facility of the National Science Foundation operated under cooperative agreement by Associated Universities, Inc. This work made use of the Swinburne University of Technology software correlator, developed as part of the Australian Major National Research Facilities Programme and operated under licence. The NASA/IPAC Extragalactic Database (NED) is operated by the Jet Propulsion Laboratory, California Institute of Technology, under contract with the National Aeronautics and Space Administration. We thank NASA for support under FERMI grant GSFC #21078/FERMI08-0051 and the NRAO for support under Student Observing Support Award GSSP10-011.

REFERENCES

- Abdo, A. A., et al. 2009, *ApJ*, 700, 597
- Abdo, A.A., et al. 2009b, *ApJ*, 707, L142
- Abdo, A. A., et al. 2010a, *ApJS*, 188, 405
- Abdo, A. A., et al. 2010b, *ApJ*, 715, 429
- Abdo, A.A., et al. 2010c, *ApJ*, 722, 520
- Abdo, A.A., et al. 2010d, *Nature*, 463, 919
- Abdo, A. A., et al. 2011, *ApJ*, 730, 101
- Adelman-McCarthy, J. K., et al. 2005, *AJ*, 129, 1755
- Adelman-McCarthy, J. K., et al. 2008, *ApJS*, 175, 297
- Agudo, I., Thum, C., Wiesenmeyer, H., & Krichbaum, T.P. 2010, *ApJS*, 189, 1
- Antón, S., Browne, I. W. A., & Marchã, M. J. 2008, *A&A*, 490, 583
- Atwood, B. W., et al. 2009, *ApJ*, 697, 1071
- Britzen, S., Brinkmann, W., Campbell, R. M., Gliozzi, M., Readhead, A. C. S., Browne, I. W. A., & Wilkinson, P. 2007, *A&A*, 476, 759
- Britzen, S., et al. 2008, *A&A*, 484, 119
- Blandford, R.D. 1976, *MNRAS*, 176, 465
- Bloom, S.D. 2008, *AJ*, 136, 1533
- Björnsson, C.I. 2010, *ApJ*, 723, 417
- Chen, R., Peng, B., Strom, R.G., & Wei, J. 2011, *MNRAS*, 412, 2433
- Ciliegi, P., Bassani, L., & Caroli, E. 1993, *ApJS*, 85, 111

- Deller, A.T., et al. 2011, *PASP*, 123, 275
- Feng, H., Rao, F., & Kaaret, P. 2010, *ApJ*, 710, L137
- Giroletti, M., Reimer, A., Fuhrmann, L., Pavlidou, V., & Richards, J. L. 2010, 2009 Fermi Symposium, eConf Proceedings C091122, arXiv:1001.5123
- Greisen, E. W. 2003, *Astrophys. Space Sci. Libr.*, 285, 109
- Healey, et al. 2007, *ApJS*, 171, 61
- Helmboldt, J. F., et al. 2007, *ApJ*, 658, 203
- Helmboldt, J.F., Taylor, G.B., Walker, R.C., & Blandford, R.D. 2008, *ApJ*, 681, 897
- Hinshaw, G., et al. 2009, *ApJS*, 180, 225
- Homan, D. C., et al. 2009, *ApJ*, 706, 1253
- Huber, P.J., & Ronchetti, E.M. 2009, *Robust Statistics* (2nd ed.; Hoboken, NJ: Wiley)
- Jorstad, S.G., et al. 2010, *ApJ*, 715, 362
- Kovalev, Y. Y., et al. 2005, *AJ*, 130, 2473
- Kovalev, Y. Y., et al. 2009, *ApJ*, 696, L17
- Linford, J. D., et al. 2011, *ApJ*, 726, 16
- Lister, M. L., et al. 2009a, *ApJ*, 138, 1874
- Lister, M. L., et al. 2009b, *AJ*, 137, 3718
- Lister, M. L., et al. 2009c, *ApJ*, 696, L22
- Lister, M.L., et al. 2011, *ApJ*, 742, 27
- Lovelace, R. 1976, *Nature*, 262, 649
- Marscher, A. P. 2006, *AIP Conf. Proc.* 856: Relativistic Jets: The Common Physics of AGN, Microquasars, and Gamma-Ray Bursts, 856, 1
- Marscher, A. P., et al. 2010, *ApJ*, 710, L126
- Meier, D.L. 2005, *Ap&SS*, 300, 55
- Mutchler, M., et al. 2007, *PASP*, 119, 851
- Ojha, R., et al. 2010a, *A&A*, 519, A45
- Ojha, R., et al. 2010b, 2009 Fermi Symposium, arXiv:1001.0059v1
- Panessa, F., & Bassani, L. 2002, *A&A*, 394, 435
- Plotkin, R. M., et al. 2008, *AJ*, 135, 2453

- Press, W. H., Flannery, B. P., Teukolsky, S. A., & Vetterlin, W. T. 1986, *Numerical Recipes: The Art of Scientific Computing* (Cambridge: Cambridge University Press)
- Pushkarev, A. B., Kovalev, Y. Y., Lister, M. L., & Savolainen, T. 2009, *A&A*, 507, L33
- Savolainen, T., et al. 2010, *A&A*, 512, A24
- Shepherd, M. C. 1997, *Astronomical Data Analysis Software and Systems VI*, ed. G. Hunt & H.E. Payne, ASP Conf. Ser., 125, 77
- Schinzel, F. K., Lobanov, A. P., Jorstad, S. G., Marscher, A. P., Taylor, G. B., & Zensus, J. A. 2010, *Fermi Meets Jansky: AGN in Radio and Gamma-Rays*, ed. T. Savolainen, E. Ros, R.W. Porcas, & J.A. Zensus, MPIfR, Bonn, Germany
- Sowards-Emmerd, D., Romani, R.W., & Michelson, P.F. 2003, *ApJ*, 590, 109
- Stawarz, L., Ostorero, L., Begelman, M.C., Moderski, R., Kataoka, J., & Wagner, S. 2008, *ApJ*, 680, 911
- Taylor, G.B., et al. 2005, *ApJS*, 159, 27
- Taylor, G.B., Gugliucci, N.E., Fabian, A.C., Sanders, J.S., Gentile, G. & Allen, S.W. 2006, *MNRAS*, 368, 1500
- Taylor, G. B. et al. 2007, *ApJ*, 671, 1355
- Tavecchio, F., Becerra-Gonzales, J., Ghisellini, G., Stamera, A., Bonnoli, G., Foschini, L., & Maraschi, L. 2011, *A&A*, 534, 86
- Urry, C. M. & Padovani, P. 1995, *PASP*, 107, 803
- de Vaucouleurs, G., de Vaucouleurs, A., Corwin, H.G., Buta, R.J., Paturel, G., & Fouque, P. 1991, *Third Reference Catalogue of Bright Galaxies (RC3)* (New York, Springer-Verlag)
- Véron-Cetty, M. P., & Véron, P. 2006, *A&A*, 455, 773
- Waggett, P.C., Warner, P.J., & Baldwin, J.E. 1977, *MNRAS*, 181, 465
- Walker, R. C., Dhawan V., Romney J. D., Kellermann K. I., & Vermeulen R.C. 2000, *ApJ*, 530, 233
- Zhou, H.Y., et al. 2007, *ApJ*, 658, L13

Table 1. Source Data

Source Name	1FGL Name	Alt. Name	RA	DEC	Opt. Type	Class	z	S ₅	LAT Flux	Δ LAT Flux	Core T _B	Open. Ang.	Δ PA
00057+3815	1FGL J0005.7+3815	B2 0003+38A	00:05:57.180	38:20:15.18	bzq	LJET	0.229	475	38.61	9.33	3.59e+10
00193+2017	1FGL J0019.3+2017	PKS 0017+200	00:19:37.850	20:21:45.61	bzb	SJET	...	680	18.93	7.63	7.18e+10
00230+4453	1FGL J0023.0+4453	B3 0020+446	00:23:35.441	44:56:35.81	bzq	LJET	1.062	120	45.43	20.21	2.53e+10	29	9
00419+2318	1FGL J0041.9+2318	PKS 0039+230	00:42:04.550	23:20:01.21	bzq	SJET	1.426	676	27.31	11.19	2.18e+10
00580+3314	1FGL J0058.0+3314	CRATES J0058+3311	00:58:32.071	33:11:17.20	bzb	PS	1.371	151	42.25	17.77	2.68e+11
01022+4223	1FGL J0102.2+4223	CRATES J0102+4214	01:02:27.151	42:14:19.00	bzq	PS	0.874	163	40.98	9.25	4.04e+11
01090+1816	1FGL J0109.0+1816	CRATES J0109+1816	01:09:08.179	18:16:07.50	bzb	LJET	0.145	55.6	17.20	7.19	1.62e+10
01120+2247	1FGL J0112.0+2247	CGRaBS J0112+2244	01:12:05.820	22:44:38.80	bzb	SJET	0.265	327	67.57	7.96	5.29e+10
01129+3207	1FGL J0112.9+3207	4C +31.03	01:12:50.330	32:08:17.59	bzq	SJET	0.603	405	139.77	9.04	4.14e+10
01138+4945	1FGL J0113.8+4945	CGRaBS J0113+4948	01:13:27.010	49:48:24.08	bzq	LJET	0.389	510	37.30	15.93	3.49e+10	7	3
01144+1327	1FGL J0114.4+1327*	CRATES J0113+1324	01:13:54.511	13:24:52.49	bzb	LJET	0.685	106	39.15	7.82	3.82e+9	20	1
01370+4751	1FGL J0137.0+4751	OC 457	01:36:58.591	47:51:29.09	bzq	SJET	0.859	3150	193.96	10.34	2.61e+11
01446+2703	1FGL J0144.6+2703	CRATES J0144+2705	01:44:33.559	27:05:03.08	bzb	LJET	...	305	40.30	8.50	4.75e+10	24	-16
02035+7234	1FGL J0203.5+7234	CGRaBS J0203+7232	02:03:33.389	72:32:53.70	bzb	LJET	...	519	63.95	28.17	8.35e+10
02045+1516	1FGL J0204.5+1516	4C +15.05	02:04:50.410	15:14:11.00	agn	LJET	0.405	1500	29.98	12.42	9.52e+10
02053+3217	1FGL J0205.3+3217	B2 0202+31	02:05:04.930	32:12:30.10	bzq	LJET	1.466	2120	45.21	19.21	1.25e+12
02112+1049	1FGL J0211.2+1049	CGRaBS J0211+1051	02:11:13.181	10:51:34.81	bzb	SJET	...	1060	41.30	8.45	1.61e+11
02178+7353	1FGL J0217.8+7353	1ES 0212+735	02:17:30.821	73:49:32.59	bzq	LJET	2.367	3950	77.11	34.06	1.28e+11
02210+3555	1FGL J0221.0+3555	B2 0218+35	02:21:05.470	35:56:13.70	bzq	CPLX	0.944	835	125.80	9.39	3.40e+9
02308+4031	1FGL J0230.8+4031	B3 0227+403	02:30:45.710	40:32:53.09	bzq	SJET	1.019	501	58.74	26.55	2.71e+10
02379+2848	1FGL J0237.9+2848	4C +28.07	02:37:52.411	28:48:09.00	bzq	LJET	1.213	2420	135.56	9.70	1.50e+11	27	3
02386+1637	1FGL J0238.6+1637	PKS 0235+164	02:38:38.930	16:36:59.29	bzb	PS	0.94	919	427.15	12.63	1.33e+11
02435+7116	1FGL J0243.5+7116	CRATES J0243+7120	02:43:30.890	71:20:17.88	bzb	SJET	...	166	25.10	8.78	9.43e+9
02454+2413	1FGL J0245.4+2413	B2 0242+23	02:45:16.860	24:05:35.20	bzq	LJET	2.243	251	41.30	17.43	2.75e+9
02580+2033	1FGL J0258.0+2033	CRATES J0258+2030	02:58:07.310	20:30:01.58	bzb	LJET	...	66.3	18.92	7.78	1.07e+10	35	-10
03106+3812	1FGL J0310.6+3812	B3 0307+380	03:10:49.879	38:14:53.81	bzq	PS	0.816	375	41.19	18.21	2.57e+11
03197+4130	1FGL J0319.7+4130	NGC 1275	03:19:48.161	41:30:42.12	agn	LJET	0.018	16200	213.59	10.69	1.23e+11
03250+3403	1FGL J0325.0+3403	B2 0321+33B	03:24:41.160	34:10:45.80	agn	LJET	0.061	357	56.29	23.97	2.15e+10
03259+2219	1FGL J0325.9+2219	CGRaBS J0325+2224	03:25:36.809	22:24:00.40	bzq	SJET	2.066	889	58.65	24.82	1.37e+11
03546+8009	1FGL J0354.6+8009	CRATES J0354+8009	03:54:46.130	80:09:28.80	agu	LJET	...	280	46.05	8.82	5.05e+10	35	-12
04335+2905	1FGL J0433.5+2905	CGRaBS J0433+2905	04:33:37.829	29:05:55.50	bzb	SJET	...	240	58.78	19.56	4.17e+10
04335+3230	1FGL J0433.5+3230	CRATES J0433+3237	04:33:40.690	32:37:12.00	bzq	SJET	2.011	59.8	17.54	7.08	4.23e+9
04406+2748	1FGL J0440.6+2748	B2 0437+27B	04:40:50.369	27:50:46.79	bzb	SJET	...	31	25.29	0.00	3.19e+9
04486+112A	1FGL J0448.6+1118*	CRATES J0448+1127	04:48:50.410	11:27:28.58	bzq	LJET	1.369	383	60.13	23.11	1.23e+10	28	-36
04486+112B	1FGL J0448.6+1118*	PKS 0446+11	04:49:07.670	11:21:28.58	bzb	SJET	1.207 ^N	1260	60.13	23.11	1.24e+11
05092+1015	1FGL J0509.2+1015	PKS 0506+101	05:09:27.461	10:11:44.59	bzq	LJET	0.621	310	53.24	22.08	4.00e+10
05100+180A	1FGL J0510.0+1800*	CRATES J0509+1806	05:09:42.910	18:06:30.31	agu	LJET	...	44.8	32.38	12.39	8.80e+9	25	3

Table 1—Continued

Source Name	1FGL Name	Alt. Name	RA	DEC	Opt. Type	Class	z	S ₅	LAT Flux	Δ LAT Flux	Core T _B	Open. Ang.	Δ PA
05100+180B	1FGL J0510.0+1800*	PKS 0507+17	05:10:02.369	18:00:41.58	bzq	LJET	0.416	441	32.38	12.39	3.63e+10	22	-3
05310+1331	1FGL J0531.0+1331	PKS 0528+134	05:30:56.419	13:31:55.09	bzq	LJET	2.07	2220	146.45	13.71	1.34e+11
06072+4739	1FGL J0607.2+4739	CGRaBS J0607+4739	06:07:23.249	47:39:47.02	bzb	LJET	...	226	32.89	13.16	3.51e+10
06127+4120	1FGL J0612.7+4120	B3 0609+413	06:12:51.190	41:22:37.42	bzb	LJET	...	296	39.74	13.60	5.21e+10
06169+5701	1FGL J0616.9+5701	CRATES J0617+5701	06:17:16.920	57:01:16.39	bzb	LJET	...	256	16.24	5.89	8.23e+10
06254+4440	1FGL J0625.4+4440	CGRaBS J0625+4440	06:25:18.259	44:40:01.60	bzb	PS	...	162	21.27	8.33	2.25e+11
06399+7325	1FGL J0639.9+7325	CGRaBS J0639+7324	06:39:21.960	73:24:58.00	bzq	LJET	1.854	612	39.52	17.33	4.73e+10	14	4
06507+2503	1FGL J0650.7+2503	1ES 0647+250	06:50:46.490	25:02:59.60	bzb	PS	0.203	21.5	16.73	5.54	3.49e+9
06544+5042	1FGL J0654.4+5042	CGRaBS J0654+5042	06:54:22.090	50:42:23.90	agu	SJET	...	240	42.02	7.63	2.31e+10
06543+4514	1FGL J0654.3+4514	B3 0650+453	06:54:23.710	45:14:23.50	bzq	PS	0.933	218	115.24	8.96	1.67e+10
07114+4731	1FGL J0711.4+4731	B3 0707+476	07:10:46.111	47:32:11.11	bzb	LJET	1.292 ^N	620	37.32	15.00	6.57e+10
07127+5033	1FGL J0712.7+5033	CGRaBS J0712+5033	07:12:43.639	50:33:22.68	bzb	PS	...	252	29.25	10.21	6.14e+10
07193+3306	1FGL J0719.3+3306	B2 0716+33	07:19:19.421	33:07:09.70	bzq	PS	0.779	383	70.34	7.31	9.91e+10
07219+7120	1FGL J0721.9+7120	CGRaBS J0721+7120	07:21:53.450	71:20:36.38	bzb	SJET	0.31	1340	149.23	8.47	7.42e+11
07253+1431	1FGL J0725.3+1431	4C +14.23	07:25:16.810	14:25:13.69	bzq	LJET	1.038	688	37.66	7.77	3.80e+10	37	-54
07382+1741	1FGL J0738.2+1741	PKS 0735+178	07:38:07.390	17:42:19.01	bzb	LJET	0.424	644	43.78	13.96	1.40e+10	31	10
07426+5444	1FGL J0742.2+5443	CRATES J0742+5444	07:42:39.7904	54:44:24.679	bzq	PS	0.723	220	59.25	24.76	4.48e+11
07464+2549	1FGL J0746.6+2548	B2 0743+25	07:46:25.8753	25:49:02.146	bzq	SJET	2.979	564	42.28	7.88	3.79e+11
07506+1235	1FGL J0750.6+1235	PKS 0748+126	07:50:52.051	12:31:04.80	bzq	LJET	0.889	3390	37.46	7.57	3.30e+11
07530+5352	1FGL J0752.8+5353	4C +54.15	07:53:01.3847	53:52:59.636	bzb	PS	0.2	485	27.01	11.32	3.76e+10
08053+6144	1FGL J0806.2+6148	CGRaBS J0805+6144	08:05:18.1778	61:44:23.704	bzq	SJET	3.033	828	36.04	8.88	5.28e+10
08096+3455	1FGL J0809.4+3455	B2 0806+35	08:09:38.8868	34:55:37.248	bzb	LJET	0.082	58.6	9.00	3.34	1.90e+10
08098+5218	1FGL J0809.5+5219	CRATES J0809+5218	08:09:49.1899	52:18:58.252	bzb	LJET	0.138	108	43.03	7.77	2.78e+9	50	20
08146+6431	1FGL J0815.0+6434	CGRaBS J0814+6431	08:14:39.1912	64:31:22.04	bzb	LJET	...	102	32.76	12.91	7.31e+10
08163+5739	1FGL J0816.7+5739	BZB J0816+5739	08:16:23.8223	57:39:09.509	bzb	CPLX	...	21.5	15.19	5.65	4.77e+8
08182+4222	1FGL J0818.2+4222	B3 0814+425	08:18:15.9995	42:22:45.408	bzb	SJET	0.53 ^N	1660	108.47	8.38	3.17e+11
08247+5552	1FGL J0825.0+5555	OJ 535	08:24:47.2364	55:52:42.662	bzq	LJET	1.417	971	62.43	8.92	3.80e+10	17	-11
08308+2410 ^M	1FGL J0830.5+2407	OJ 248	08:30:52.0855	24:10:59.818	bzq	SJET	0.94	1110	65.29	8.21	4.14e+11
08338+4224	1FGL J0834.4+4221	B3 0830+425	08:33:53.8852	42:24:01.859	bzq	SJET	0.249	249	31.44	7.80	3.90e+10
08422+7054	1FGL J0842.2+7054	4C +71.07	08:41:24.360	70:53:42.22	bzq	LJET	2.218	1680	61.94	8.92	9.87e+9	9	-19
08499+4852	1FGL J0849.9+4852	CRATES J0850+4854	08:50:00.530	48:54:52.60	agu	LJET	...	60.1	29.87	6.99	1.20e+9	54	121
08548+2006 ^M	1FGL J0854.8+2006	OJ 287	08:54:48.8741	20:06:30.639	bzb	SJET	0.306	2380	63.31	13.83	3.17e+11
08566+2057	1FGL J0856.6+2103*	CRATES J0850+2057	08:56:39.7398	20:57:43.426	bzq	LJET	0.539 ^N	45.1	39.89	17.57	1.28e+10	16	10
08569+2111	1FGL J0856.6+2103*	OJ 290	08:56:57.2424	21:11:43.64	bzq	LJET	2.098	365	39.89	17.57	8.24e+9
09055+1356	1FGL J0905.5+1356	CRATES J0905+1358	09:05:34.990	13:58:06.31	agu	SJET	...	48.5	18.39	7.21	7.33e+9
09106+3329	1FGL J0910.7+3332	Ton 1015	09:10:37.0354	33:29:24.418	bzb	LJET	0.354	130	22.76	9.04	4.04e+10
09121+4126	1FGL J0912.3+4127	B3 0908+416B	09:12:11.6174	41:26:09.356	bzq	LJET	2.563	132	18.51	7.61	3.95e+9

Table 1—Continued

Source Name	1FGL Name	Alt. Name	RA	DEC	Opt. Type	Class	z	S ₅	LAT Flux	Δ LAT Flux	Core T _B	Open. Ang.	Δ PA
158+2933	1FGL J0915.7+2931	B2 0912+29	09:15:52.4014	29:33:23.982	bzb	LJET	...	80	22.64	8.34	1.30e+10
209+4441	1FGL J0920.9+4441	B3 0917+449	09:20:58.4599	44:41:53.988	bzq	LJET	2.19	1020	242.01	9.44	3.59e+10	44	-159
216+6215	1FGL J0919.6+6216	OK 630	09:21:36.2322	62:15:52.185	bzq	LJET	1.446	1410	35.59	7.95	1.59e+11
235+4125	1FGL J0923.2+4121	B3 0920+416	09:23:31.3037	41:25:27.429	agn	LJET	0.028	220	40.61	10.01	2.97e+10	10	1
238+2815	1FGL J0924.2+2812	B2 0920+28	09:23:51.522	28:15:24.966	bzq	PS	0.744	899	44.39	19.61	1.95e+11
292+5013	1FGL J0929.4+5000	CRATES J0929+5013	09:29:15.4401	50:13:35.982	bzb	LJET	0.37039 ^N	430	21.40	9.29	4.81e+10
341+3926	1FGL J0934.5+3929	CGRaBS J0934+3926	09:34:06.674	39:26:32.125	bzb	PS	0.044 ^N	108	19.72	7.73	2.89e+10
372+5008	1FGL J0937.7+5005	CGRaBS J0937+5008	09:37:12.3257	50:08:52.082	bzq	PS	0.276	324	52.33	11.77	1.05e+11
418+2728	1FGL J0941.2+2722	CGRaBS J0941+2728	09:41:48.1135	27:28:38.818	bzq	PS	1.306	235	18.15	7.24	1.46e+10
456+5754	1FGL J0945.6+5754	CRATES J0945+5757	09:45:42.240	57:57:47.70	bzb	LJET	0.229	42.9	17.96	7.22	1.64e+10
466+1012	1FGL J0946.6+1012	CRATES J0946+1017	09:46:35.071	10:17:06.11	bzq	SJET	1.007	245	28.22	11.71	2.42e+10
496+1752	1FGL J0949.8+1757*	CRATES J0949+1752	09:49:39.7634	17:52:49.432	bzq	LJET	0.693	207	18.85	0.00	1.50e+11
498+1757	1FGL J0949.8+1757*	CRATES J0950+1804	09:50:00.310	18:04:18.70	agu	SJET	0.69327 ^N	37.2	18.85	0.00	1.43e+9
565+6938	1FGL J0956.5+6938	M 82	09:55:52.726	69:40:45.77	sbq	PS	0.000677 ^N	14	38.40	16.23	3.39e+9
568+2515	1FGL J0956.9+2513	B2 0954+25A	09:56:49.8747	25:15:16.047	bzq	PS	0.712	645	28.07	11.59	7.88e+9
576+5522	1FGL J0957.7+5523	4C +55.17	09:57:38.1837	55:22:57.74	bzq	LJET	0.896	580	106.45	7.43	9.88e+8	68	-1
001+6539	1FGL J1000.1+6539	CGRaBS J0958+6533	09:58:47.251	65:33:54.79	bzb	LJET	0.367	1450	28.21	11.72	5.07e+11
127+2440	1FGL J1012.7+2440	CRATES J1012+2439	10:12:41.381	24:39:23.40	bzq	SJET	1.805	63.9	49.66	6.81	5.56e+9
150+4926	1FGL J1015.1+4927	1ES 1011+496	10:15:04.1336	49:26:00.704	bzb	LJET	0.2	201	63.31	6.16	7.98e+9
330+4116	1FGL J1033.2+4116	B3 1030+415	10:33:03.7086	41:16:06.234	bzq	LJET	1.117	1290	29.30	6.86	2.22e+12
338+6051	1FGL J1033.8+6048	CGRaBS J1033+6051	10:33:51.427	60:51:07.342	bzq	SJET	1.401	188	50.15	7.02	1.55e+10
377+5711	1FGL J1037.7+5711	CRATES J1037+5711	10:37:44.311	57:11:55.61	bzb	PS	...	61.8	30.14	10.02	1.73e+10
431+2408	1FGL J1043.1+2404	B2 1040+24A	10:43:09.0347	24:08:35.43	bzb	SJET	0.56	738	18.02	6.92	1.26e+11
487+8054	1FGL J1048.7+8054	CGRaBS J1044+8054	10:44:23.071	80:54:39.38	bzq	LJET	1.26	727	57.94	8.73	3.32e+10	3	-10
485+7239	1FGL J1048.5+7239	CRATES J1047+7238	10:47:47.520	72:38:13.02	agu	LJET	...	61	44.18	19.09	1.60e+10
488+7145	1FGL J1048.8+7145	CGRaBS J1048+7143	10:48:27.619	71:43:35.90	bzq	PS	1.15	1170	59.88	26.71	1.09e+11
586+5628	1FGL J1058.6+5628	CGRaBS J1058+5628	10:58:37.7261	56:28:11.18	bzb	LJET	0.143	159	56.29	6.84	1.93e+10
044+3812	1FGL J1104.4+3812	Mkn 421	11:04:27.3145	38:12:31.794	bzb	LJET	0.03	262	170.63	7.25	8.35e+10
061+2812	1FGL J1106.5+2809	CRATES J1106+2812	11:06:07.2592	28:12:47.045	agu	PS	0.847 ^N	227	34.63	15.03	2.25e+11
126+3446	1FGL J1112.8+3444	CRATES J1112+3446	11:12:38.7673	34:46:39.124	bzq	LJET	1.949	197	33.70	13.80	6.37e+10
171+2013	1FGL J1117.1+2013	CRATES J1117+2014	11:17:06.259	20:14:07.40	bzb	LJET	0.138	36.5	11.66	3.57	1.28e+10
240+2336	1FGL J1123.9+2339	OM 235	11:24:02.7109	23:36:45.876	bzb	SJET	...	362	23.95	9.65	6.96e+10
366+7009	1FGL J1136.6+7009	Mkn 180	11:36:26.410	70:09:27.32	bzb	LJET	0.045	136	13.12	4.46	2.51e+10
421+1547	1FGL J1141.8+1549	CRATES J1142+1547	11:42:07.7378	15:47:54.202	agu	LJET	...	139	12.87	5.19	9.15e+10	28	5
469+3958	1FGL J1146.8+4004	B2 1144+40	11:46:58.2987	39:58:34.307	bzq	PS	1.089	603	46.91	20.17	2.85e+11
503+2417	1FGL J1150.2+2419	B2 1147+24	11:50:19.2146	24:17:53.852	bzb	LJET	0.2	621	29.11	11.81	4.47e+10	20	-8
514+5859	1FGL J1151.6+5857	CRATES J1151+5859	11:51:24.6554	58:59:17.552	bzb	SJET	...	61.7	18.22	7.12	3.88e+9

Table 1—Continued

Source Name	1FGL Name	Alt. Name	RA	DEC	Opt. Type	Class	z	S ₅	LAT Flux	Δ LAT Flux	Core T _B	Open. Ang.	Δ PA
540+6022	1FGL J1152.1+6027	CRATES J1154+6022	11:54:04.5339	60:22:20.785	...	PS	...	232	46.21	20.76	3.93e+11
595+2914 ^M	1FGL J1159.4+2914	4C +29.45	11:59:31.8338	29:14:43.823	bzq	LJET	0.729	1250	115.40	7.84	2.36e+12
030+6031	1FGL J1202.9+6032	CRATES J1203+6031	12:03:03.5094	60:31:19.129	agn	LJET	0.065	145	44.79	20.07	2.75e+10
089+5441	1FGL J1209.3+5444	CRATES J1208+5441	12:08:54.2583	54:41:58.19	bzq	PS	1.344	252	35.45	15.20	2.28e+11
093+4119	1FGL J1209.4+4119	B3 1206+416	12:09:22.7851	41:19:41.36	bzb	LJET	0.377 ^N	131	22.25	9.57	2.91e+10
098+1810	1FGL J1209.7+1806	CRATES J1209+1810	12:09:51.7649	18:10:06.796	bzq	SJET	0.845	140	19.72	7.97	3.19e+10
178+3007	1FGL J1217.7+3007	B2 1215+30	12:17:52.0838	30:07:00.625	bzb	LJET	0.13	261	83.01	31.55	7.36e+10
215+7106	1FGL J1221.5+7106	CRATES J1220+7105	12:20:03.631	71:05:31.09	bzq	SJET	0.451	183	10.07	3.84	9.96e+10
201+3431	1FGL J1220.2+3432	CGRaBS J1220+3431	12:20:08.2902	34:31:21.711	bzb	LJET	0.643 ^N	129	11.03	4.65	1.90e+10
215+2813	1FGL J1221.5+2814	W Com	12:21:31.6936	28:13:58.497	bzb	LJET	0.102	320	76.04	11.97	3.64e+10
248+8044	1FGL J1224.8+8044	CRATES J1223+8040	12:23:40.500	80:40:04.30	bzb	LJET	...	450	25.48	10.12	4.01e+10	27	-1
248+4335	1FGL J1225.8+4336*	B3 1222+438	12:24:51.5074	43:35:19.276	agu	LJET	1.07491 ^N	207	36.15	15.51	3.15e+10
249+2122 ^M	1FGL J1224.7+2121	4C +21.35	12:24:54.4600	21:22:46.438	bzq	LJET	0.435	746	69.70	7.78	3.97e+11	81	5
269+4340	1FGL J1225.8+4336*	B3 1224+439	12:26:57.9051	43:40:58.438	bzq	SJET	2.002	85	36.15	15.51	8.58e+9
302+2518	1FGL J1230.4+2520	ON 246	12:30:14.0935	25:18:07.145	bzb	LJET	0.135	206	27.43	11.46	1.97e+10	33	-3
316+2850	1FGL J1231.6+2850	B2 1229+29	12:31:43.579	28:47:49.81	bzb	LJET	0.236	86.3	25.44	8.13	1.33e+10	17	7
3431+3627	1FGL J1243.1+3627	B2 1240+36	12:43:12.739	36:27:43.99	bzb	SJET	1.0654 ^N	59.6	24.30	9.36	8.77e+9
3483+5820	1FGL J1248.2+5820	CGRaBS J1248+5820	12:48:18.784	58:20:28.725	bzb	LJET	0.847 ^N	124	61.70	6.81	3.85e+10	36	2
3531+5301	1FGL J1253.0+5301	CRATES J1253+5301	12:53:11.9232	53:01:11.741	bzb	LJET	...	240	35.44	6.32	2.91e+10	10	3
3579+3229	1FGL J1258.3+3227	B2 1255+32	12:57:57.2313	32:29:29.321	bzq	LJET	0.806	467	21.96	0.00	3.49e+10
3630+2433	1FGL J1303.0+2433	CRATES J1303+2433	13:03:03.2143	24:33:55.684	bzb	PS	0.993 ^N	134	36.84	6.88	1.52e+11
3660+7852	1FGL J1306.0+7852	CRATES J1305+7854	13:05:00.019	78:54:35.71	agu	SJET	...	213	17.53	6.82	1.82e+10
3683+3546	1FGL J1308.5+3550	CGRaBS J1308+3546	13:08:23.7095	35:46:37.16	bzq	SJET	1.055	309	41.59	16.49	3.25e+11
3692+1156	1FGL J1309.2+1156	4C +12.46	13:09:33.931	11:54:24.59	bzb	LJET	...	629	29.66	12.32	9.56e+9	33	8
3104+3220 ^M	1FGL J1310.6+3222	B2 1308+32	13:10:28.6618	32:20:43.790	bzq	LJET	0.997	1240	135.55	8.98	6.57e+11	25	-32
3127+4828	1FGL J1312.4+4827	CGRaBS J1312+4828	13:12:43.3508	48:28:30.928	bzq	PS	0.501	66.7	31.29	12.84	1.62e+9
3147+2348	1FGL J1314.7+2346	CRATES J1314+2348	13:14:43.8021	23:48:26.701	bzb	LJET	...	123	35.58	15.30	2.22e+10
3176+3425	1FGL J1317.8+3425	B2 1315+34A	13:17:36.4935	34:25:15.921	bzq	LJET	1.05	260	18.93	7.43	4.47e+10
3211+2216	1FGL J1321.1+2214	CGRaBS J1321+2216	13:21:11.2041	22:16:12.098	bzq	SJET	0.943	244	34.18	14.92	2.14e+10
3213+8310	1FGL J1321.3+8310	CRATES J1321+8316	13:21:45.590	83:16:13.40	agu	LJET	1.024 ^N	232	27.88	11.62	1.32e+10	9	-9
3270+2210 ^M	1FGL J1326.6+2213	B2 1324+22	13:27:00.8577	22:10:50.150	bzq	SJET	1.4	1120	54.09	11.78	1.22e+12
3307+5202	1FGL J1331.0+5202	CGRaBS J1330+5202	13:30:42.5962	52:02:15.448	agn	LJET	0.688	148	41.52	0.00	4.50e+10
3327+4722	1FGL J1332.9+4728	B3 1330+476	13:32:45.2413	47:22:22.653	bzq	PS	0.669	298	32.08	14.24	1.30e+11
3338+5057	1FGL J1333.2+5056	CLASS J1333+5057	13:33:53.7823	50:57:35.914	agu	PS	1.362 ^N	48.4	64.33	27.63	1.46e+10
3455+4452	1FGL J1345.4+4453	B3 1343+451	13:45:33.1685	44:52:59.581	bzq	SJET	2.534	333	52.18	21.04	2.11e+11
3508+3034	1FGL J1351.0+3035	B2 1348+30B	13:50:52.7333	30:34:53.582	bzq	SJET	0.714	251	14.81	5.25	3.29e+10
3533+1434	1FGL J1353.3+1434	PKS 1350+148	13:53:22.841	14:35:39.30	bzb	LJET	...	177	24.77	10.48	9.44e+9	32	29

Table 1—Continued

Source Name	1FGL Name	Alt. Name	RA	DEC	Opt. Type	Class	z	S ₅	LAT Flux	Δ LAT Flux	Core T _B	Open. Ang.	Δ PA
3581+7646	1FGL J1358.1+7646	CGRaBS J1357+7643	13:57:55.370	76:43:21.00	bzq	SJET	1.585	425	40.70	17.83	8.58e+10
3590+5544	1FGL J1359.1+5539	CRATES J1359+5544	13:59:05.7379	55:44:29.362	bzq	PS	1.014	108	37.91	16.61	6.36e+10
4270+2348	1FGL J1426.9+2347	PKS 1424+240	14:27:00.3942	23:48:00.045	bzb	CPLX	...	199	69.51	7.92	1.21e+10
4340+4203	1FGL J1433.9+4204	B3 1432+422	14:34:05.6956	42:03:16.01	bzq	SJET	1.24	131	25.17	10.63	1.50e+10
4366+2321	1FGL J1436.9+2314	PKS 1434+235	14:36:40.9873	23:21:03.297	bzq	LJET	1.545	600	24.69	10.78	2.79e+11
4388+3710	1FGL J1438.7+3711*	B2 1436+37B	14:38:53.6095	37:10:35.408	bzq	LJET	2.401	263	33.44	15.00	2.31e+11
4387+3711	1FGL J1438.7+3711*	CRATES J1439+3712	14:39:20.580	37:12:02.81	bzq	LJET	1.021	33.3	33.44	15.00	9.52e+9
4438+2457	1FGL J1443.8+2457	PKS 1441+25	14:43:56.890	25:01:44.51	bzq	LJET	0.939	286	20.05	7.96	1.15e+11
4509+5201	1FGL J1451.0+5204	CLASS J1450+5201	14:50:59.9877	52:01:11.7	bzb	PS	...	37.5	33.61	14.31	2.25e+10
4544+5124	1FGL J1454.6+5125	CRATES J1454+5124	14:54:27.1247	51:24:33.734	bzb	LJET	1.08 ^N	80.2	50.54	22.17	5.83e+9
5044+1029	1FGL J1504.4+1029	PKS 1502+106	15:04:24.979	10:29:39.19	bzq	LJET	1.839	1030	1061.22	14.67	3.54e+10	56	-18
5061+3730	1FGL J1505.8+3725	B2 1504+37	15:06:09.5287	37:30:51.128	bzq	LJET	0.674	630	31.13	12.90	8.54e+10	11	3
5169+1932	1FGL J1516.9+1928	PKS 1514+197	15:16:56.7985	19:32:13.01	bzb	LJET	1.07 ^N	662	35.06	15.62	2.27e+11
5197+4216	1FGL J1519.7+4216	B3 1518+423	15:20:39.720	42:11:11.51	bzq	PS	0.484	40.8	20.75	8.72	1.09e+10
5221+3144	1FGL J1522.1+3143	B2 1520+31	15:22:09.9947	31:44:14.427	bzq	CPLX	1.487	462	411.49	10.60	1.12e+11
5396+2744	1FGL J1539.7+2747	CGRaBS J1539+2744	15:39:39.141	27:44:38.288	bzq	SJET	2.19	145	13.50	4.90	9.70e+10
5429+6129	1FGL J1542.9+6129	CRATES J1542+6129	15:42:56.9464	61:29:55.358	bzb	LJET	...	97.8	65.53	6.88	2.38e+10
5534+1255	1FGL J1553.4+1255	PKS 1551+130	15:53:32.700	12:56:51.68	bzq	LJET	1.308	658	119.49	13.66	1.21e+10	29	-157
5557+1111	1FGL J1555.7+1111	PG 1553+113	15:55:43.039	11:11:24.40	bzb	SJET	0.36	160	77.62	22.73	6.35e+10
6046+5714	1FGL J1604.3+5710	CGRaBS J1604+5714	16:04:37.3568	57:14:36.668	bzq	LJET	0.72	374	54.28	23.42	1.01e+10	3	14
6071+1551	1FGL J1607.1+1552	4C +15.54	16:07:06.4276	15:51:34.495	agn	LJET	0.496	322	33.90	7.75	3.19e+10	27	4
6090+1031	1FGL J1609.0+1031	4C +10.45	16:08:46.200	10:29:07.80	bzq	LJET	1.226	1120	61.34	9.82	4.12e+10
6136+3412 ^M	1FGL J1613.5+3411	B2 1611+34	16:13:41.0633	34:12:47.903	bzq	LJET	1.397	2960	22.67	9.88	3.58e+10
6160+4632	1FGL J1616.1+4637	CRATES J1616+4632	16:16:03.7689	46:32:25.239	bzq	PS	0.95	74.2	37.69	16.18	4.16e+10
6302+5220	1FGL J1630.2+5220	CRATES J1630+5221	16:30:43.150	52:21:38.59	bzb	PS	...	27.3	19.32	7.35	1.59e+9
6354+8228	1FGL J1635.4+8228	NGC 6251	16:32:31.980	82:32:16.40	agn	LJET	0.025	637	45.51	18.77	1.41e+10	1	2
6377+4717	1FGL J1637.9+4707	4C +47.44	16:37:45.1338	47:17:33.822	bzq	LJET	0.74	673	35.84	8.79	7.56e+10
6410+1143	1FGL J1641.0+1143	CRATES J1640+1144	16:40:58.889	11:44:04.20	agn	LJET	0.078	115	47.36	20.81	7.65e+9
6475+4950	1FGL J1647.4+4948	CGRaBS J1647+4950	16:47:34.9142	49:50:00.586	agn	LJET	0.047	154	33.29	8.54	2.02e+10
6568+6012	1FGL J1656.9+6017	CRATES J1656+6012	16:56:48.2475	60:12:16.455	bzq	PS	0.623	323	18.12	7.82	7.16e+10
7001+6830	1FGL J1700.1+6830	CGRaBS J1700+6830	17:00:09.300	68:30:07.02	bzq	PS	0.301	372	55.99	7.32	7.28e+10
7096+4318	1FGL J1709.6+4320	B3 1708+433	17:09:41.0876	43:18:44.547	bzq	LJET	1.027	140	42.84	17.10	2.19e+10
7192+1745	1FGL J1719.2+1745	PKS 1717+177	17:19:13.049	17:45:06.41	bzb	SJET	0.137	642	44.76	15.61	1.66e+11
7225+1012	1FGL J1722.5+1012	CRATES J1722+1013	17:22:44.580	10:13:35.80	bzq	SJET	0.732	386	59.14	26.13	1.93e+10
7240+4004	1FGL J1724.0+4002	B2 1722+40	17:24:05.4301	40:04:36.457	agn	LJET	1.049	435	47.16	8.97	3.32e+11
7250+1151	1FGL J1725.0+1151	CGRaBS J1725+1152	17:25:04.339	11:52:15.49	bzb	SJET	0.018 ^N	63.3	54.96	23.25	4.47e+10
7274+4530	1FGL J1727.3+4525	B3 1726+455	17:27:27.6472	45:30:39.743	bzq	SJET	0.714	1050	39.28	7.93	1.68e+12

Table 1—Continued

Source Name	1FGL Name	Alt. Name	RA	DEC	Opt. Type	Class	z	S ₅	LAT Flux	Δ LAT Flux	Core T _B	Open. Ang.	Δ PA
7283+5013	1FGL J1727.9+5010	I Zw187	17:28:18.6238	50:13:10.48	bzb	LJET	0.055	133	28.67	12.02	6.88e+9	11	31
7308+3716	1FGL J1730.8+3716	CRATES J1730+3714	17:30:47.050	37:14:55.10	bzb	SJET	...	54.9	24.08	9.56	1.91e+9
7343+3857	1FGL J1734.4+3859	B2 1732+38A	17:34:20.5821	38:57:51.446	bzq	PS	0.976	872	99.48	10.85	1.22e+11
7425+5945	1FGL J1742.1+5947	CRATES J1742+5945	17:42:32.0074	59:45:06.729	bzb	LJET	...	118	27.81	7.02	1.58e+10	1	-1
7442+1934	1FGL J1744.2+1934	1ES 1741+196	17:43:57.830	19:35:08.99	bzb	SJET	0.083	154	15.54	6.15	1.12e+10
7485+7004	1FGL J1748.5+7004	CGRaBS J1748+7005	17:48:32.839	70:05:50.78	bzb	CPLX	0.77	615	31.49	12.02	2.88e+10
7490+4321	1FGL J1749.0+4323	B3 1747+433	17:49:00.3604	43:21:51.287	bzb	LJET	...	373	35.44	14.39	6.46e+10
7566+5524	1FGL J1756.6+5524*	CRATES J1757+5523	17:57:28.279	55:23:11.90	bzb	LJET	0.065	40.7	27.79	12.00	4.04e+9
8004+7827	1FGL J1800.4+7827	CGRaBS J1800+7828	18:00:45.679	78:28:04.01	bzb	LJET	0.68	2370	64.41	7.67	1.28e+11	12	-8
8070+6945	1FGL J1807.0+6945	3C 371	18:06:50.681	69:49:28.09	bzb	LJET	0.051	1200	75.93	12.26	4.46e+10	6	14
8096+2908	1FGL J1809.6+2908	CRATES J1809+2910	18:09:45.389	29:10:19.88	bzb	SJET	...	96.9	21.61	8.26	1.32e+11
8134+3141	1FGL J1813.4+3141	B2 1811+31	18:13:35.210	31:44:17.59	bzb	LJET	0.117	81.3	30.48	11.57	1.31e+10
8240+5651	1FGL J1824.0+5651	4C +56.27	18:24:07.070	56:51:01.51	bzb	LJET	0.664 ^N	1060	64.59	10.22	1.82e+11
8485+3224	1FGL J1848.5+3224	B2 1846+32A	18:48:22.099	32:19:02.60	bzq	LJET	0.798	322	74.19	15.38	3.55e+10
8493+6705	1FGL J1849.3+6705	CGRaBS J1849+6705	18:49:16.080	67:05:41.71	bzq	LJET	0.657	1310	227.47	9.47	3.84e+11
8525+4853	1FGL J1852.5+4853	CGRaBS J1852+4855	18:52:28.550	48:55:47.50	bzq	PS	1.25	420	51.36	22.81	7.41e+11
9030+5539	1FGL J1903.0+5539	CRATES J1903+5540	19:03:11.611	55:40:38.39	bzb	LJET	...	180	37.53	15.16	2.49e+10	35	-4
9416+7214	1FGL J1941.6+7214	CRATES J1941+7221	19:41:26.981	72:21:42.19	agu	SJET	...	157	66.46	29.70	2.18e+10
0000+6508	1FGL J2000.0+6508	1ES 1959+650	19:59:59.849	65:08:54.71	bzb	LJET	0.049	213	71.92	8.60	2.31e+10	39	2
0019+7040	1FGL J2001.9+7040	CRATES J2001+7040	20:01:33.950	70:40:25.82	agu	LJET	...	36.5	27.18	10.17	5.63e+9
0060+7751	1FGL J2006.0+7751	CGRaBS J2005+7752	20:05:31.001	77:52:43.21	bzb	LJET	0.342	904	51.58	22.83	9.70e+10
0091+7228	1FGL J2009.1+7228	4C +72.28	20:09:52.301	72:29:19.39	bzb	LJET	...	775	46.83	13.78	1.62e+10
0204+7608	1FGL J2020.4+7608	CGRaBS J2022+7611	20:22:35.590	76:11:26.20	bzb	LJET	...	774	45.59	19.42	1.19e+11	33	27
0315+1219	1FGL J2031.5+1219	PKS 2029+121	20:31:55.001	12:19:41.30	bzb	SJET	1.215 ^N	1080	50.42	21.03	4.74e+11
0354+1100	1FGL J2035.4+1100	PKS 2032+107	20:35:22.339	10:56:06.79	bzq	LJET	0.601	522	74.93	14.31	1.36e+11
0497+1003	1FGL J2049.7+1003*	PKS 2047+098	20:49:45.859	10:03:14.40	agu	LJET	...	698	58.69	25.99	6.07e+10
1155+2937	1FGL J2115.5+2937	B2 2113+29	21:15:29.419	29:33:38.41	bzq	LJET	1.514	705	39.17	11.71	7.26e+9
1161+3338	1FGL J2116.1+3338	B2 2114+33	21:16:14.520	33:39:20.41	bzb	LJET	...	49.5	38.92	15.69	4.46e+9
1209+1901	1FGL J2120.9+1901	OX 131	21:21:00.610	19:01:28.31	bzq	LJET	2.18	363	43.68	17.31	2.25e+10	21	5
1434+1742	1FGL J2143.4+1742	OX 169	21:43:35.539	17:43:48.68	bzq	SJET	0.211	728	184.60	10.49	1.52e+11
1525+1734	1FGL J2152.5+1734	PKS 2149+17	21:52:24.821	17:34:37.81	bzb	SJET	0.871	495	20.25	7.86	1.51e+10
1574+3129	1FGL J2157.4+3129	B2 2155+31	21:57:28.819	31:27:01.40	bzq	SJET	1.486	479	53.99	10.54	3.57e+11
2035+1726	1FGL J2203.5+1726	PKS 2201+171	22:03:26.890	17:25:48.29	bzq	LJET	1.076	692	93.40	8.59	6.52e+10
22121+2358	1FGL J2212.1+2358	PKS 2209+236	22:12:05.971	23:55:40.58	bzq	LJET	1.125	902	21.37	8.40	1.30e+11
22171+2423	1FGL J2217.1+2423	B2 2214+24B	22:17:00.830	24:21:46.01	bzb	LJET	0.505	550	42.39	8.32	3.30e+11
22193+1804	1FGL J2219.3+1804	CGRaBS J2219+1806	22:19:14.090	18:06:35.60	bzq	SJET	1.071	169	25.49	10.40	4.80e+10
22362+2828	1FGL J2236.2+2828	B2 2234+28A	22:36:22.469	28:28:57.40	bzq	SJET	0.795	1500	84.96	8.23	2.62e+11

Table 1—Continued

Source Name	1FGL Name	Alt. Name	RA	DEC	Opt. Type	Class	z	S ₅	LAT Flux	Δ LAT Flux	Core T _B	Open. Ang.	Δ PA
22440+2021	1FGL J2244.0+2021	CRATES J2243+2021	22:43:54.739	20:21:03.82	bzb	LJET	...	60.5	38.41	14.31	1.51e+10
22501+3825	1FGL J2250.1+3825	B3 2247+381	22:50:05.750	38:24:37.19	bzb	SJET	0.119	56.5	26.04	10.72	5.33e+9
22517+4030	1FGL J2251.7+4030	CRATES J2251+4030	22:51:59.770	40:30:58.21	bzb	SJET	...	63.2	46.51	19.73	9.07e+9
22539+1608	1FGL J2253.9+1608	3C 454.3	22:53:57.751	16:08:53.59	bzq	LJET	0.859	11200	1355.47	17.05	5.91e+11	36	24
23073+1452	1FGL J2307.3+1452	CGRaBS J2307+1450	23:07:34.001	14:50:17.99	bzb	LJET	0.503 ^N	50.7	24.64	9.21	2.32e+10
23110+3425	1FGL J2311.0+3425	B2 2308+34	23:11:05.330	34:25:10.88	bzq	LJET	1.817	808	53.68	9.52	5.80e+10
23220+3208	1FGL J2322.0+3208	B2 2319+31	23:21:54.950	32:04:07.61	bzq	LJET	1.489	475	40.48	17.44	2.32e+11
23216+2726	1FGL J2321.6+2726	4C +27.50	23:21:59.861	27:32:46.39	bzq	LJET	1.253	941	41.26	18.15	4.25e+10
23226+3435	1FGL J2322.6+3435	CRATES J2322+3436	23:22:44.011	34:36:13.90	bzb	PS	0.098	27.3	34.87	0.00	6.68e+9
23252+3957	1FGL J2325.2+3957	B3 2322+396	23:25:17.870	39:57:36.50	bzb	SJET	...	139	27.66	8.30	1.24e+10

Note. — Col. (1): Source name: if name starts with 'J' it is a VIPS or MOJAVE source; if name starts with 'F' it is a new source. Col. (2): 1FGL source name. Col. (3): Alternate source name. Col. (4): Right Ascension (J2000). Col. (5): Declination (J2000). Col. (6): Optical Type (1LAC): bzb = BL Lac object, bzq = FSRQ, agn = non-blazar AGN, agu = AGN of uncertain type, sbg = starburst galaxy. Col. (7): Automated Source Classification: LJET = Long Jet, SJET = Short Jet, PS = Point Source, CPLX = Complex. Col. (8): Redshift, from 1LAC (Abdo et al. 2010b) except where specified. Col. (9): Total VLBA flux density at 5 GHz. Col. (10): γ -ray flux in units of 10^{-9} photons $\text{cm}^{-2} \text{s}^{-1}$ for 100 MeV–1 TeV. Col. (11): Error in the γ -ray flux in the same units as the flux. Col. (12): Core Brightness Temperature as measured by automated program (Helmboldt et al 2007). Col. (13): Opening Angle in degrees. Col. (14): Change in jet position angle in degrees.

^NMOJAVE source. For more data, visit the MOJAVE website <http://www.physics.purdue.edu/astro/MOJAVE/MOJAVEIItable.html> or see Lister et al. (2009b)

†Indicates a LAT source which is associated with multiple radio sources with high ($\geq 80\%$) probability in 1LAC

Redshift obtained from NED

Table 2. Source Classifications

LAT/non-LAT	Opt Type	LJET	SJET	PS	CPLX	CSO	Unidentified
LAT-detected							
	BL Lacs	55 (58%)	25 (26%)	12 (13%)	3 (3%)
	FSRQs	54 (50%)	30 (28%)	21 (20%)	2 (2%)
	AGN/Other	21 (70%)	5 (17%)	4 (13%)
non-LAT-detected							
	BL Lacs	11 (46%)	7 (29%)	6 (25%)
	FSRQs	188 (39%)	121 (25%)	136 (28%)	2 ($\sim 1\%$)	30 (6%)	2 ($\sim 1\%$)
	AGN/Other	214 (42%)	98 (19%)	111 (21%)	11 (2%)	71 (14%)	10 (2%)

Note. — LJET = long jet, SJET = short jet, PS = point source, CPLX = complex, CSO = compact symmetric object candidate

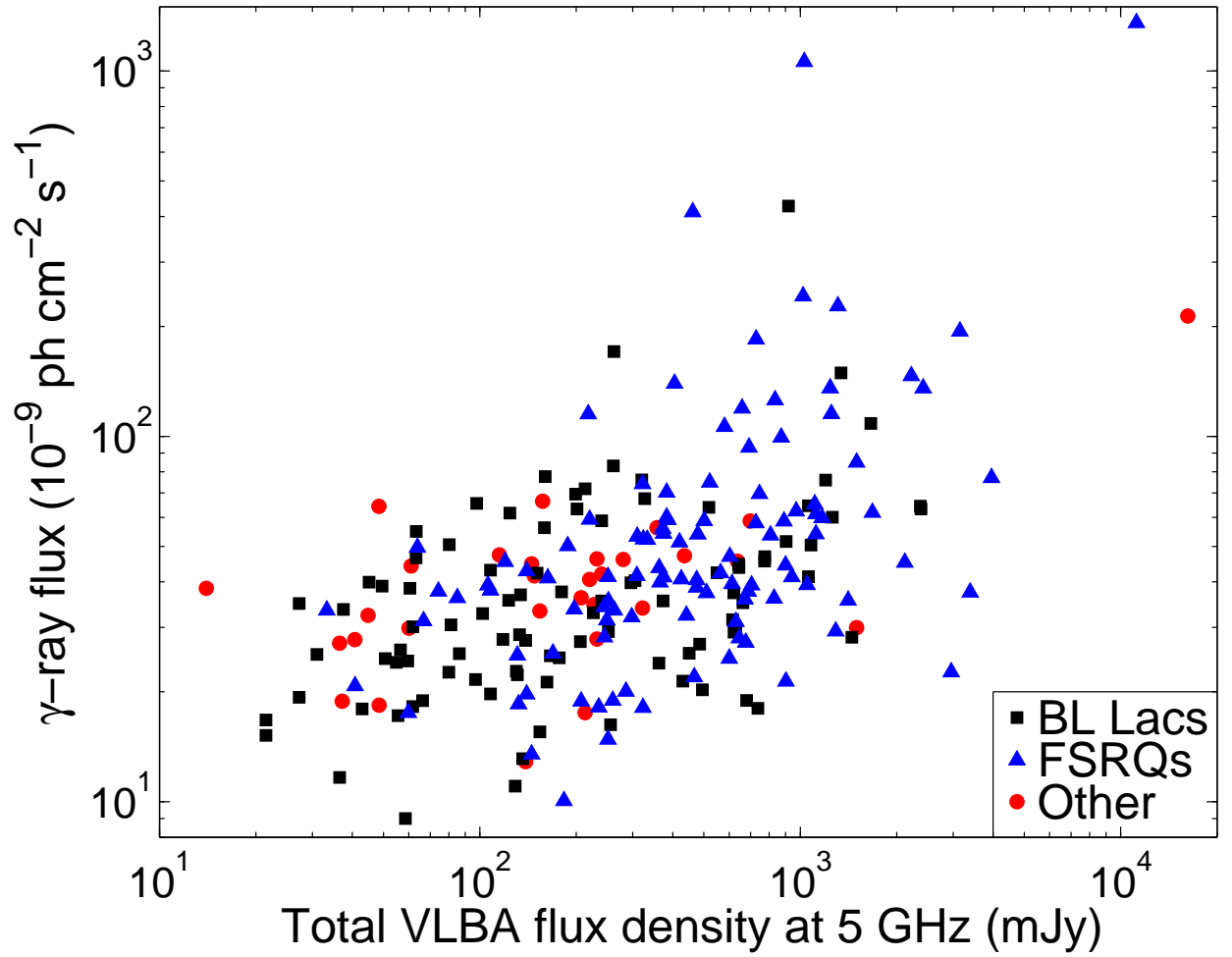


Fig. 1.—: LAT γ -ray flux (100 MeV - 100 GeV) vs. total VLBA radio flux density at 5 GHz. The γ -ray fluxes are in units of 10^{-9} photons cm $^{-2}$ s $^{-1}$. The black squares are BL Lacs, the blue triangles are FSRQs, and the red circles are radio galaxies and unclassified objects. Error bars are omitted for ease of viewing.

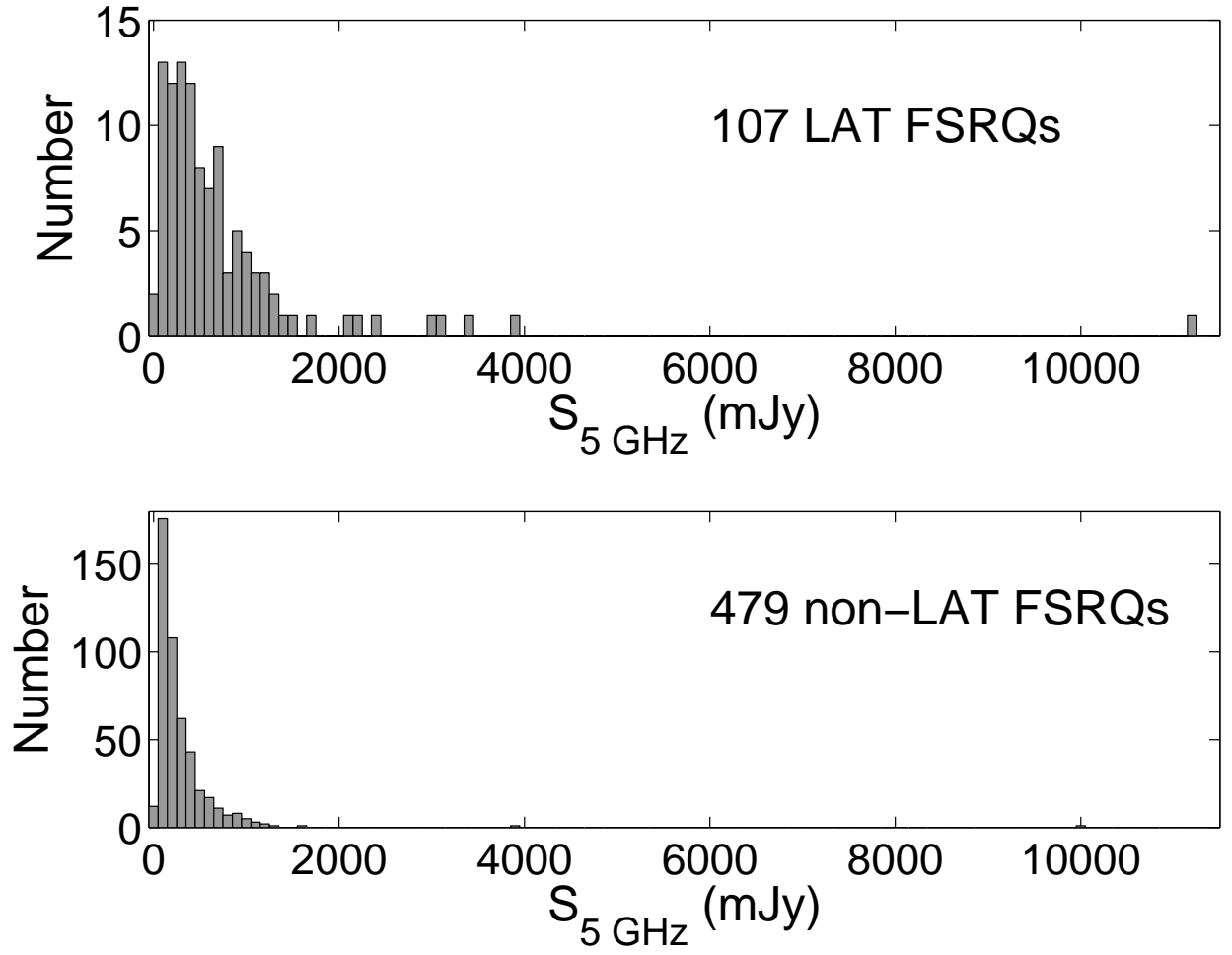


Fig. 2.—: Distributions of LAT (top) and non-LAT (bottom) FSRQ total VLBA flux density at 5 GHz.

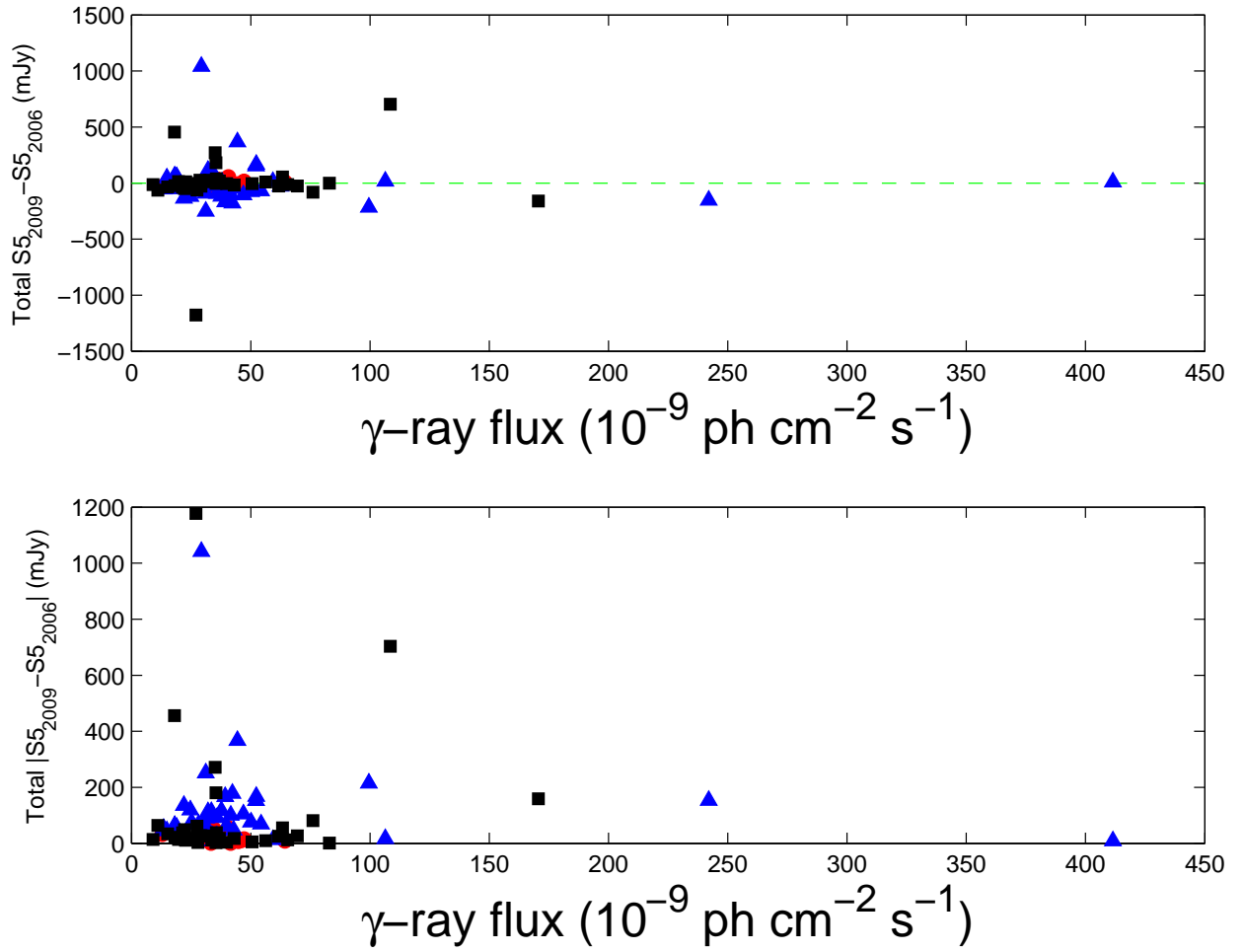


Fig. 3.— Top: Difference in total flux density at 5 GHz (current - archival) versus total LAT flux. Bottom: Absolute value of the difference in total flux density (current - archival) versus total LAT flux. Black squares are BL Lac objects, blue triangles are FSRQs, and red circles are AGN/other.

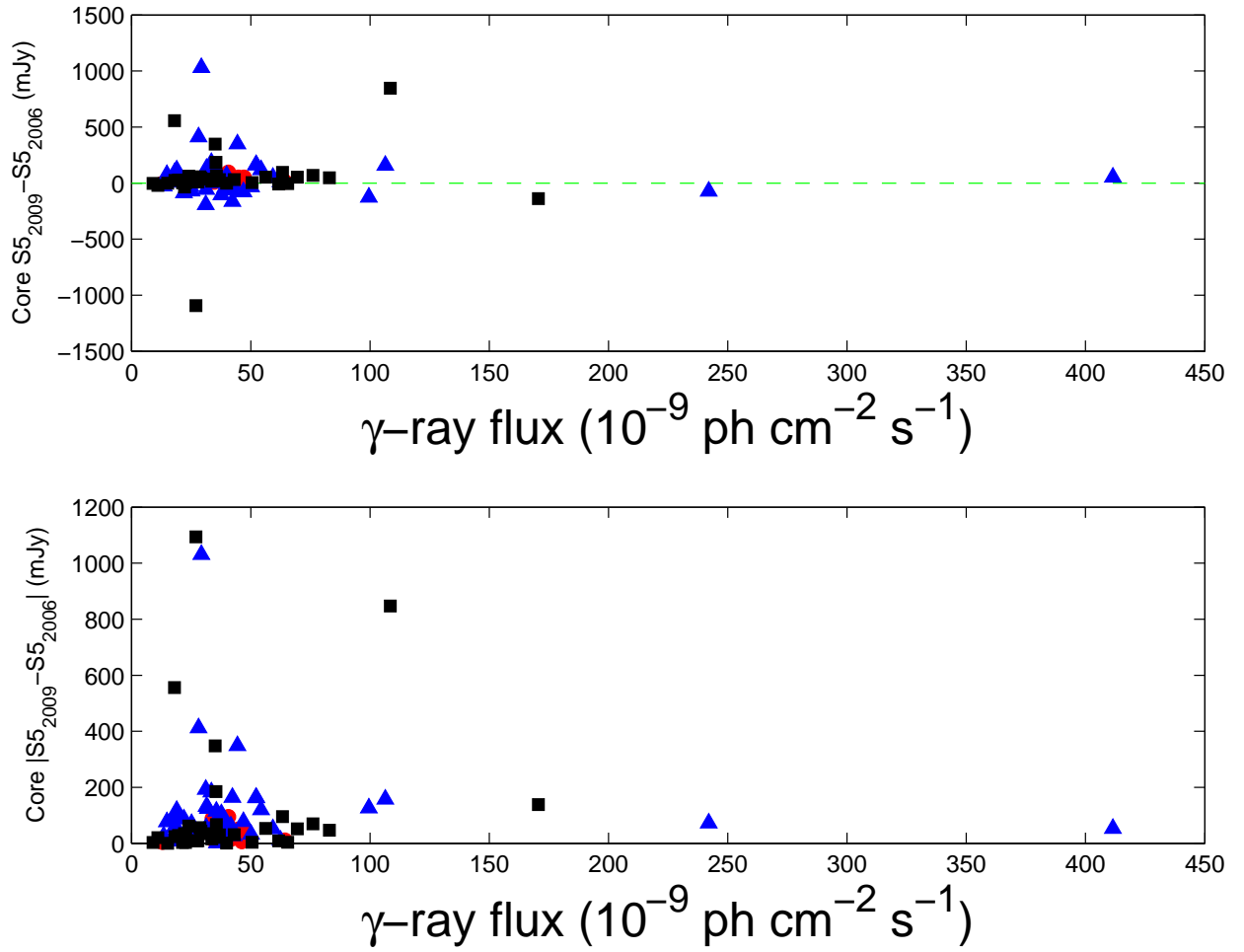


Fig. 4.— Top: Difference in core flux density at 5 GHz (current - archival) versus total LAT flux. Bottom: Absolute value of the difference in core flux density (current - archival) versus total LAT flux. Black squares are BL Lac objects, blue triangles are FSRQs, and red circles are AGN/other.

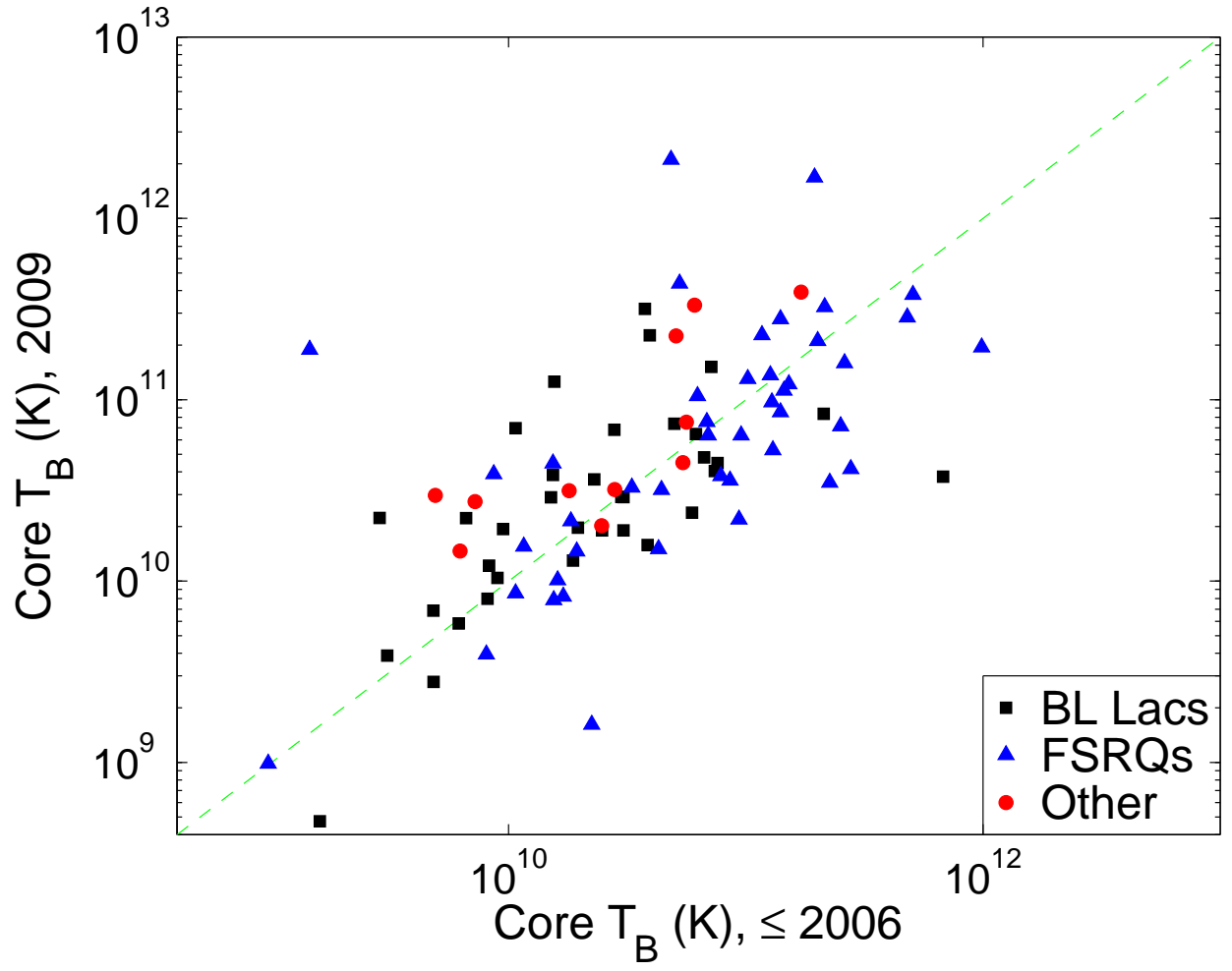


Fig. 5.—: Core brightness temperatures, current data (2009-2010) vs. archival data (prior to or during 2006).

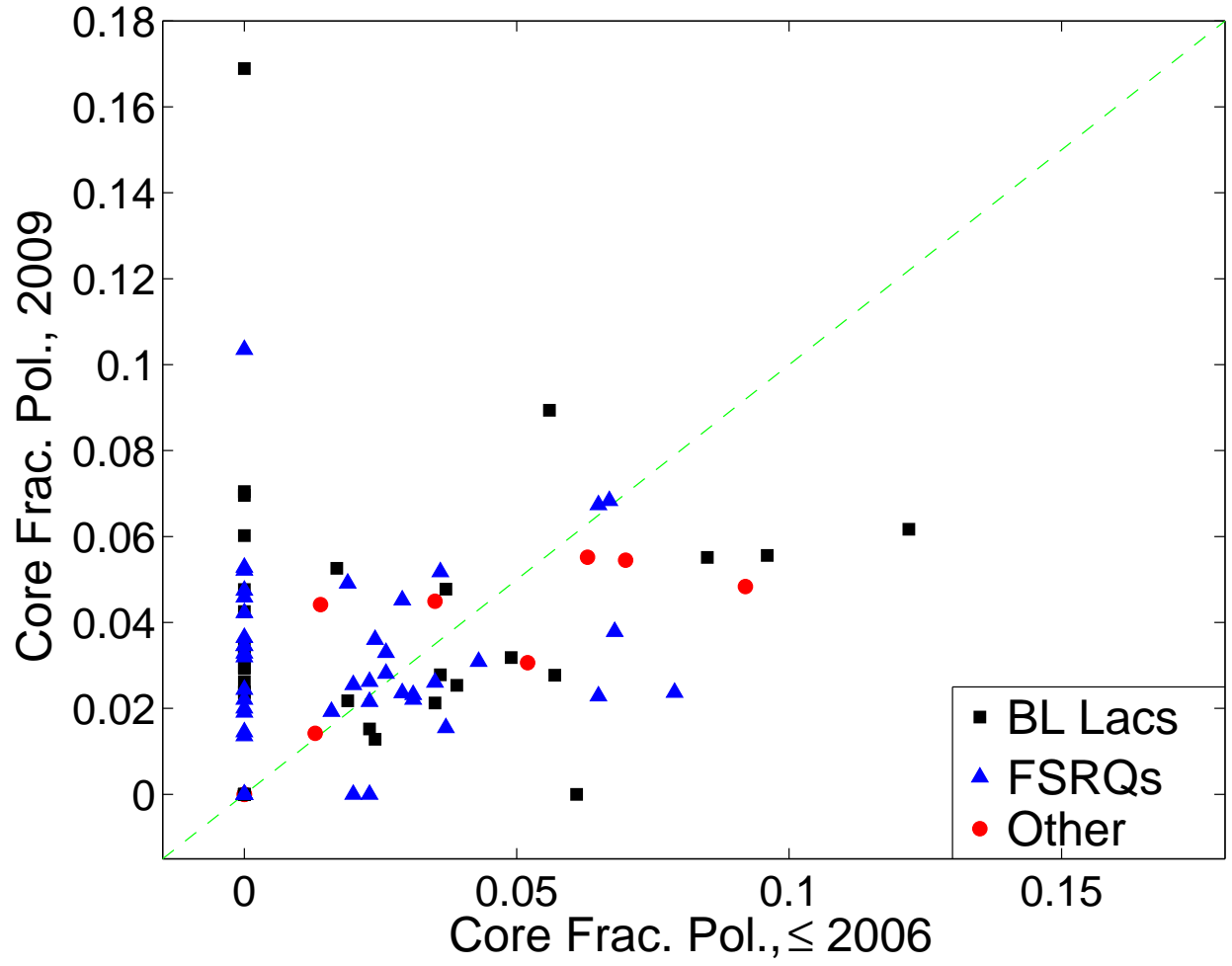


Fig. 6.—: Core fractional polarization at 5 GHz, current data (2009-2010) vs. archival data (prior to or during 2006).

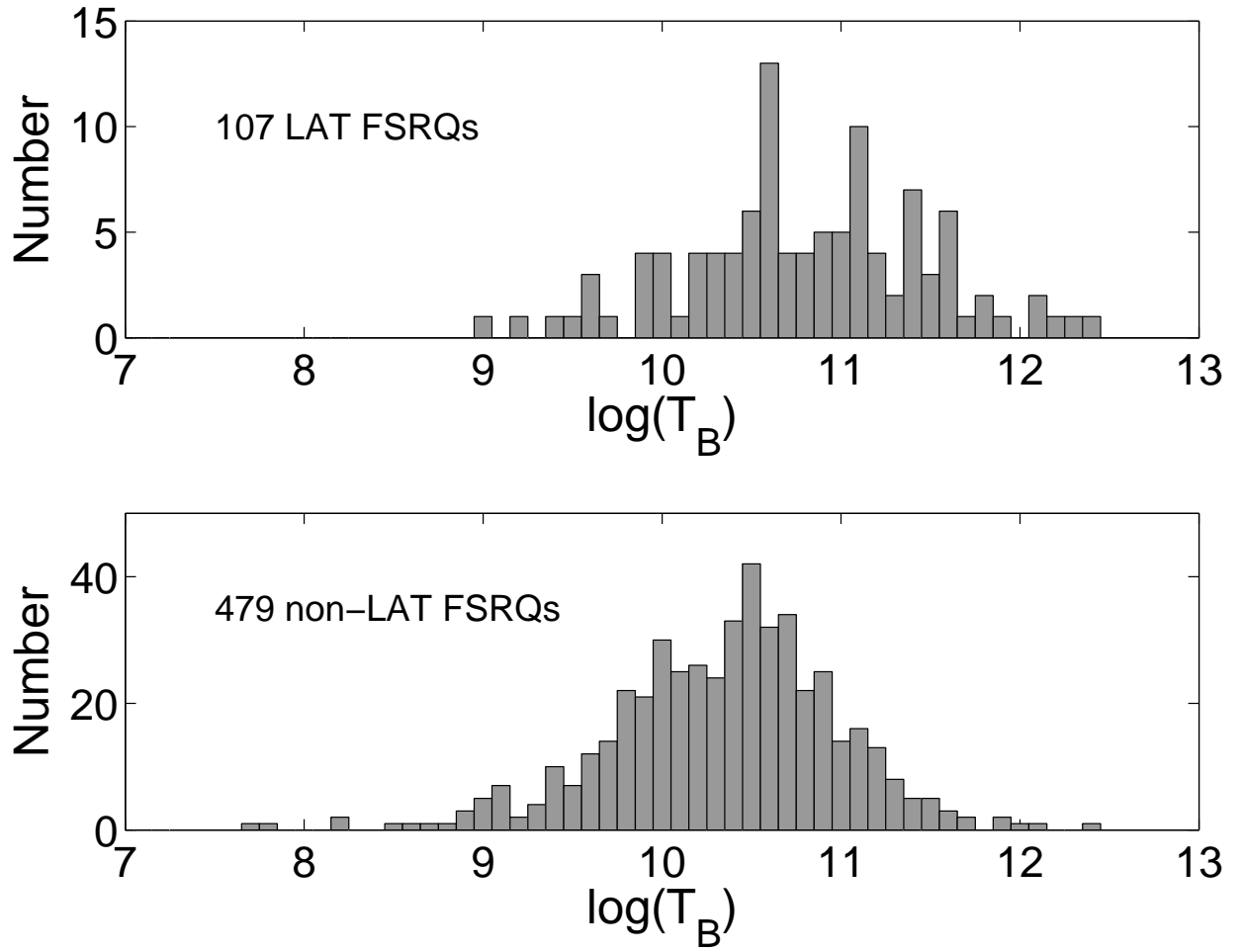


Fig. 7.—: The distributions of core brightness temperatures for LAT-detected FSRQs (top) compared to the distributions of core brightness temperature for non-LAT FSRQs in VIPS (bottom).

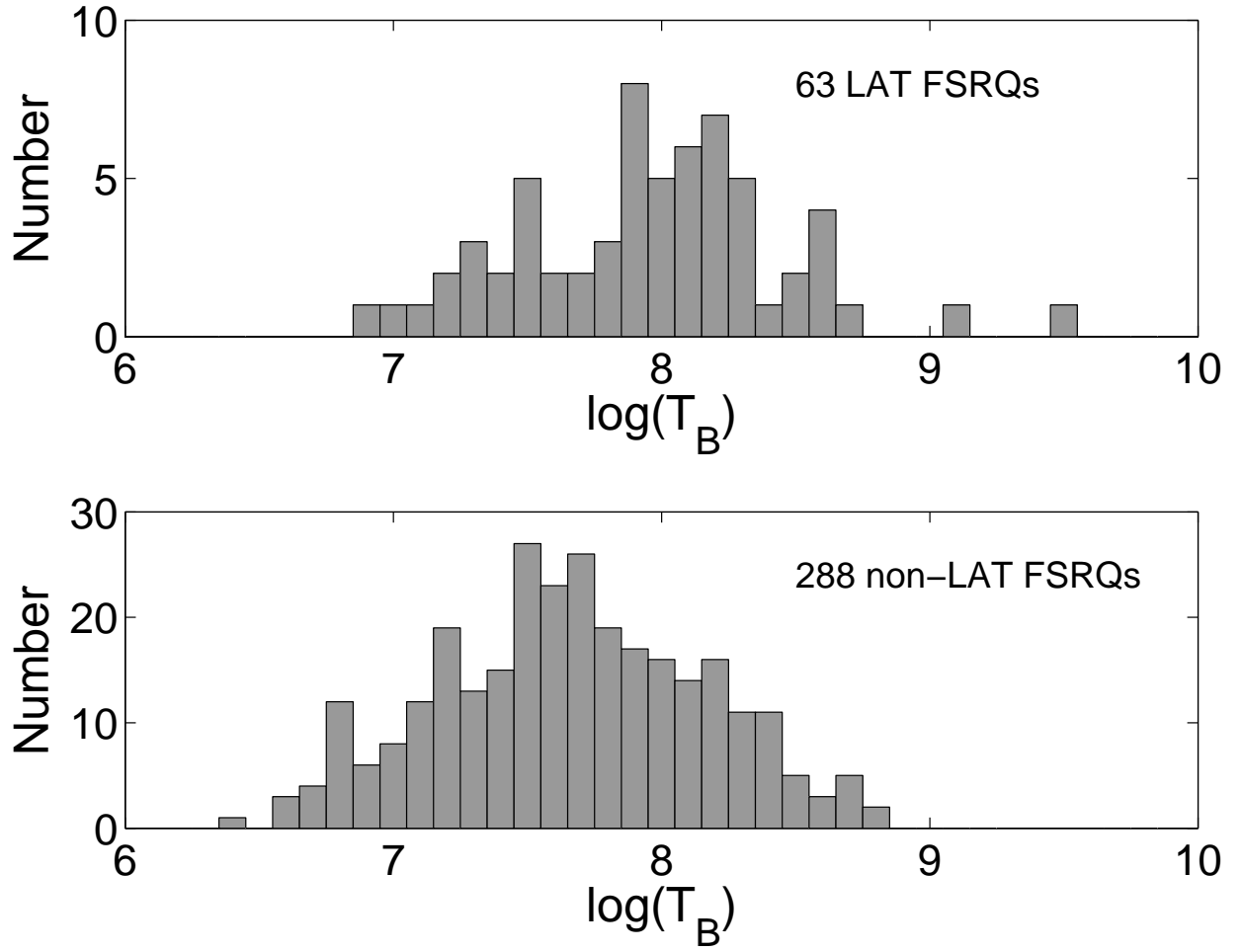


Fig. 8.—: The distributions for jet brightness temperatures for LAT (top) and non-LAT (bottom) FSRQs.

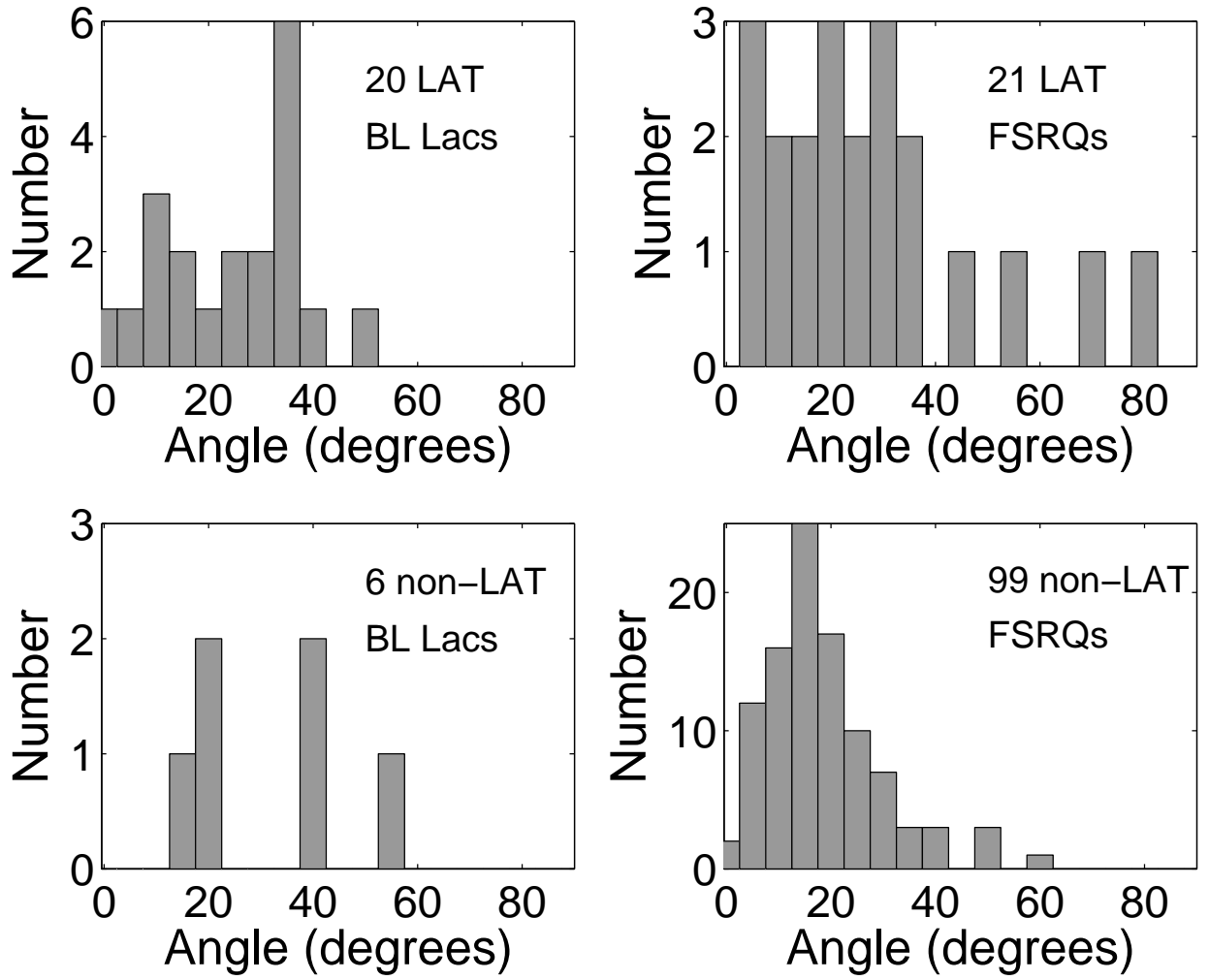


Fig. 9.—: The distributions of apparent opening angles for BL Lacs (left) and FSRQs (right) for both the LAT-detected (top) and non-LAT detected (bottom) sources.

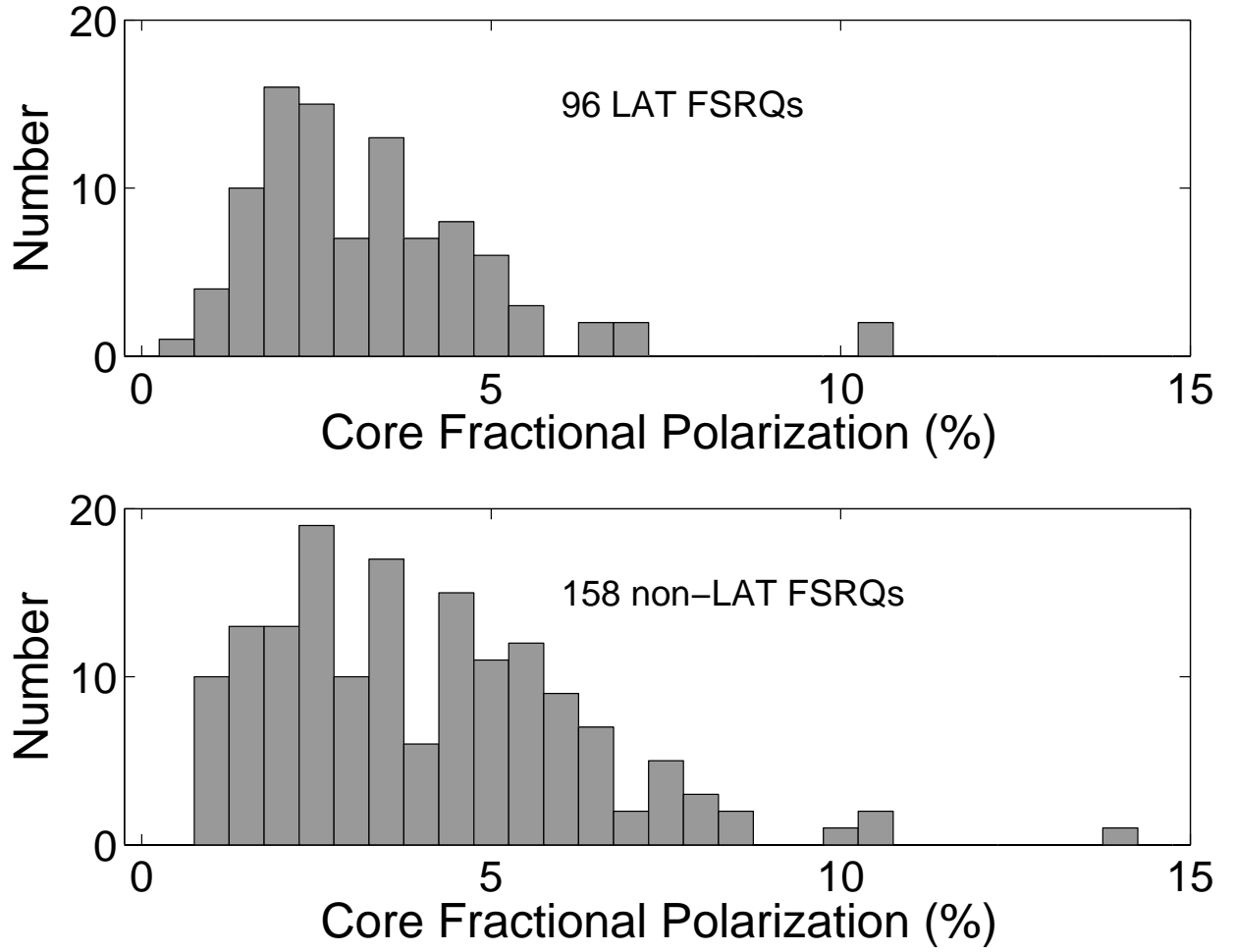


Fig. 10.—: The distribution of core fractional polarization for LAT (top) and non-LAT (bottom) FSRQs.

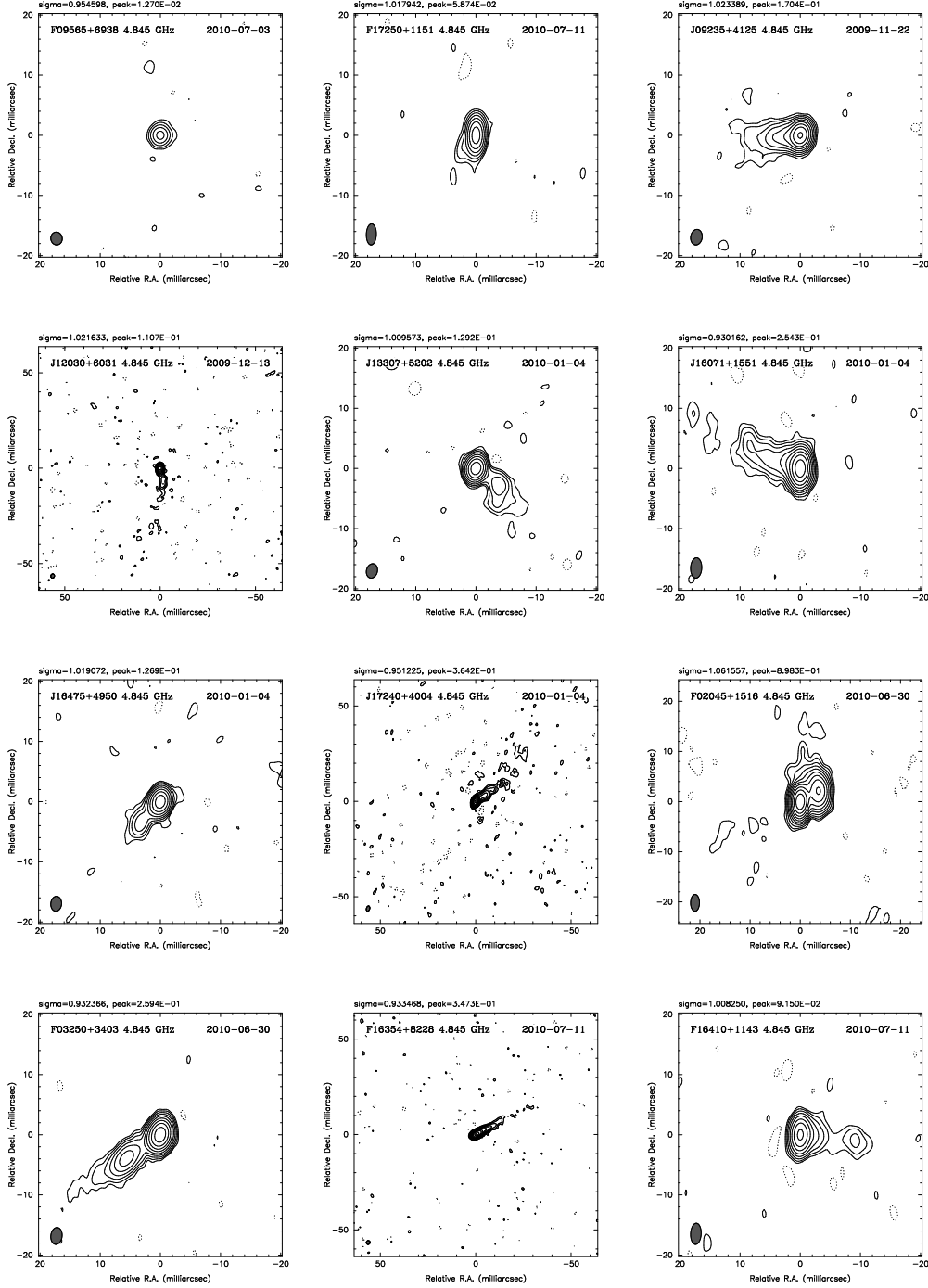


Fig. 11.—: Contour maps of sources in Section 7. All data were taken with the VLBA at 5 GHz. Bottom contours are all at 0.6 mJy/beam, except for F02045+1516 which has a bottom contour of 1 mJy/beam. The restoring beam is shown as an ellipse in the lower left corner.

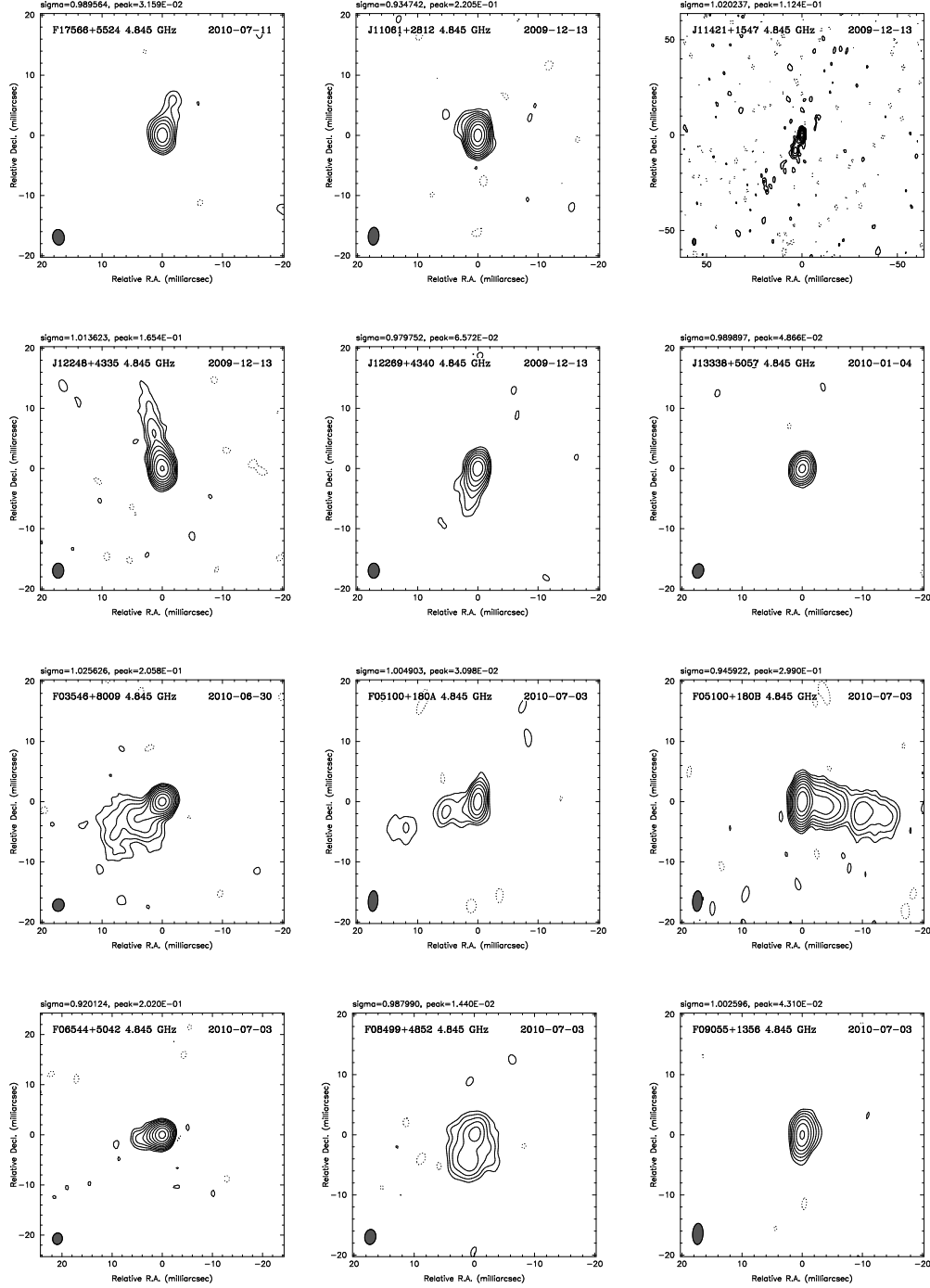


Fig. 11.—: Contour maps of sources in Section 7. All data were taken with the VLBA at 5 GHz. Bottom contours are all at 0.6 mJy/beam. The restoring beam is shown as an ellipse in the lower left corner.

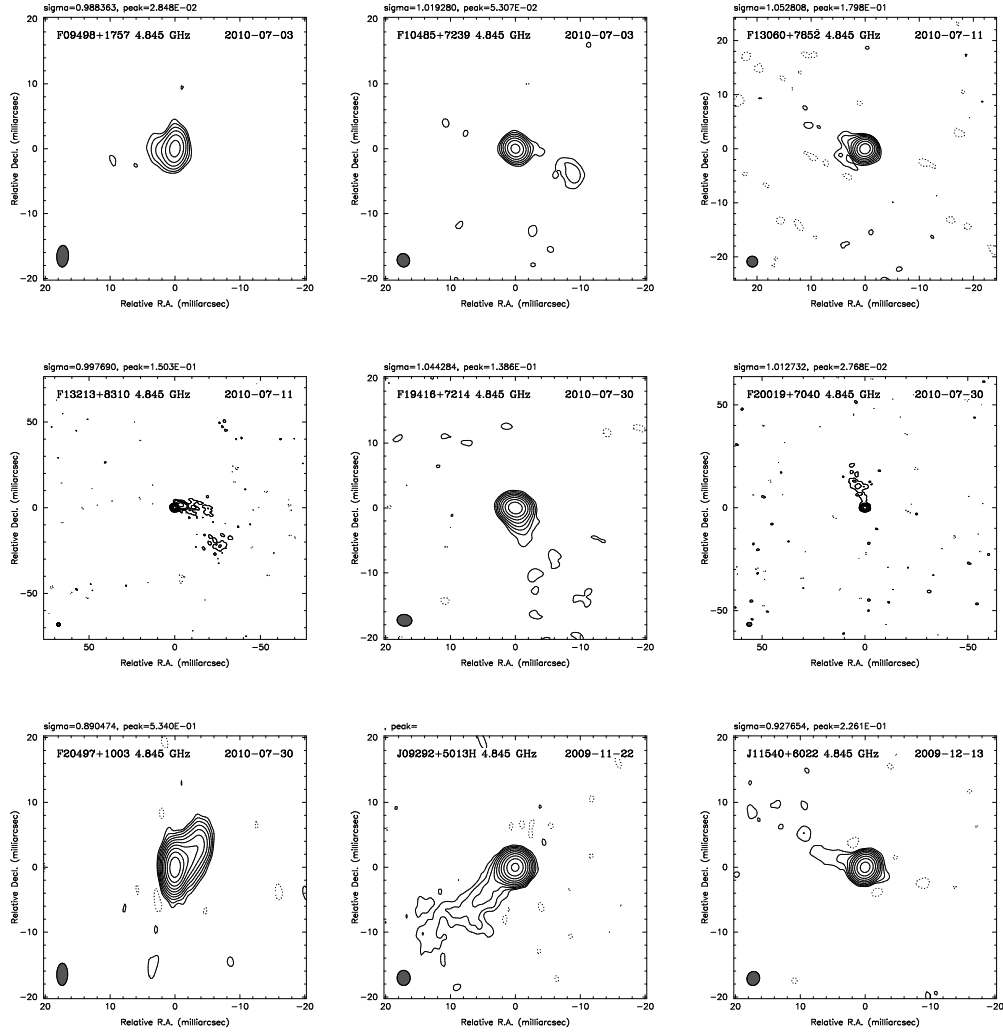


Fig. 11.—: Contour maps of sources in Section 7. All data were taken with the VLBA at 5 GHz. Bottom contours are all at 0.6 mJy/beam, except for F13060+7852 and F13213+8310 which have bottom contours of 0.8 mJy/beam. The restoring beam is shown as an ellipse in the lower left corner.

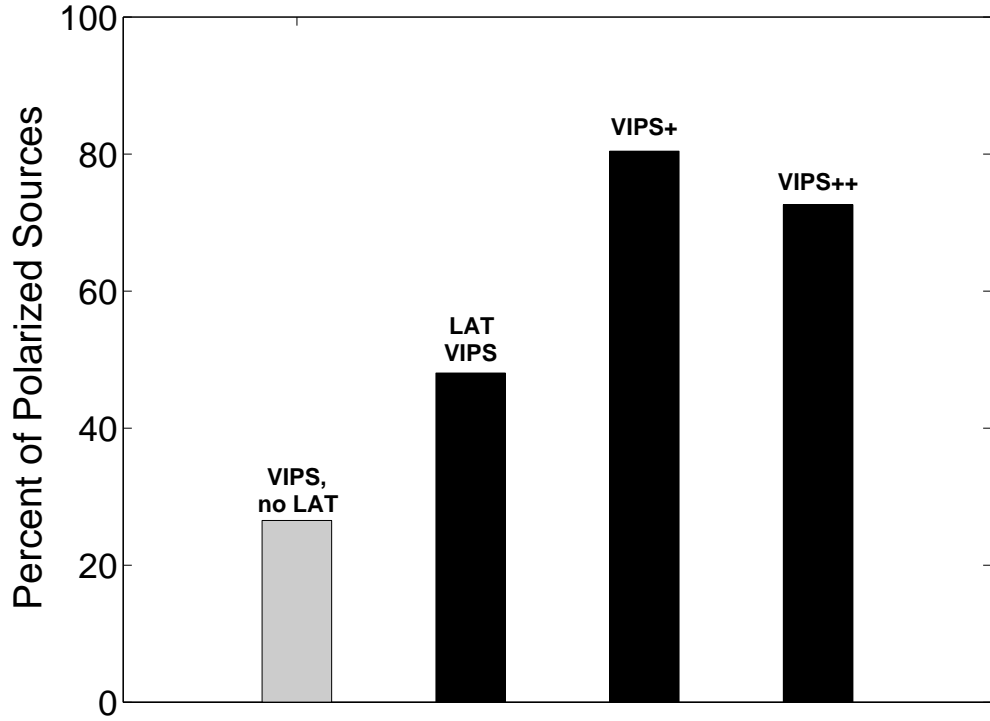


Fig. 12.—: The percentage of sources found to be polarized in various VLBI samples including VIPS (observations made prior to or during 2006), VIPS+ (2nd epoch VIPS observations made contemporaneously with Fermi observations, 2009-2010), and VIPS++ (contemporaneous observations of additional LAT blazars, 2010). Gray indicates the sample with no LAT-detected sources, black indicates LAT samples.